Dynamic regulation of T_{FH} selection during the germinal centre reaction

https://doi.org/10.1038/s41586-021-03187-x

Received: 9 March 2020

Accepted: 24 December 2020

Published online: 03 February 2021

Check for updates

Julia Merkenschlager[1]✉, Shlomo Finkin[1], Victor Ramos[1], Julian Kraft[1], Melissa Cipolla[1], Carla R. Nowosad[2], Harald Hartweger[1], Wenzhu Zhang[3], Paul Dominic B. Olinares[3], Anna Gazumyan[1,4], Thiago Y. Oliveira[1], Brian T. Chait[3] & Michel C. Nussenzweig[1,4]

The germinal centre is a dynamic microenvironment in which B cells that express high-affinity antibody variants produced by somatic hypermutation are selected for clonal expansion by limiting the numbers of T follicular helper cells[1,2]. Although much is known about the mechanisms that control the selection of B cells in the germinal centre, far less is understood about the clonal behaviour of the T follicular helper cells that help to regulate this process. Here we report on the dynamic behaviour of T follicular helper cell clones during the germinal centre reaction. We find that, similar to germinal centre B cells, T follicular helper cells undergo antigen-dependent selection throughout the germinal centre reaction that results in differential proliferative expansion and contraction. Increasing the amount of antigen presented in the germinal centre leads to increased division of T follicular helper cells. Competition between T follicular helper cell clones is mediated by the affinity of T cell receptors for peptide–major-histocompatibility-complex ligands. T cells that preferentially expand in the germinal centre show increased expression of genes downstream of the T cell receptor, such as those required for metabolic reprogramming, cell division and cytokine production. These dynamic changes lead to marked remodelling of the functional T follicular helper cell repertoire during the germinal centre reaction.

Humoral immunity and effective vaccination necessitate the development of high-affinity antibody-producing cells in germinal centres (GCs). These responses are regulated by T follicular helper (T_{FH}) cells that express BCL6, the chemokine receptor CXCR5, high levels of PD-1, and B cell trophic cytokines, each of which is required to orchestrate the GC reaction. Within GCs, limiting numbers of T_{FH} cells interact with and select B cells on the basis of their ability to bind, internalize and present antigen as peptide complexed with major histocompatibility proteins (pMHC). Thus, the selection of B cells requires competition for limiting T_{FH} cell signals[3–7].

B cells in the GC divide rapidly, hypermutate their antibody genes, and undergo affinity-based selection during the GC reaction. Productive contacts between T_{FH} cells and GC B cells leads to increases in the T_{FH} cell intracellular calcium concentration and the production of B cell trophic interleukins. Whether these signalling events also lead to T_{FH} cell proliferation, clonal selection and expansion within the GC has not been investigated[8]. To examine the kinetics of T_{FH} cell development in response to antigens during the GC reaction, we immunized mice with 4-hydroxyl-3-nitrophenylacetyl-ovalbumin (OVA) (NP-OVA) (Fig. 1a, Extended Data Fig. 1a). Consistent with other reports[1,9,10], T_{FH} cells ($CD4^+$, $CD62^{low}$, $CD44^{high}$, $CXCR5^{high}$, $PD1^{high}$, $BCL6^+$) were first detected 4 to 5 days after immunization and expanded exponentially thereafter, reaching a peak at days 7–10, before contracting by day 21 (Fig. 1b).

Unlike most other effector T cells, T_{FH} cells are thought to be largely quiescent, in part because limiting the size of the GC T_{FH} cell pool is required to maintain stringent B cell selection and prevent autoimmunity[7,11–15]. To explore whether T_{FH} cells continue to divide once they have seeded the GC reaction, we tracked cell division by the incorporation of the thymidine analogue 5-ethynyl-2´-deoxyuridine (EdU) and intranuclear expression of Ki67 (Fig. 1c). We found that the proliferative profile of T_{FH} cells paralleled that of GC B cells and was significantly ($P = 0.001$ or $P < 0.0001$) different from naive quiescent T cells. Proliferation peaked early, with a subsequent decrease to lower but significant levels of proliferation that persisted throughout the 19-day observation period (Fig. 1c). Similarly, 2–8% of T_{FH} cells in chronic GCs in mesenteric lymph nodes and Peyer's patches incorporated EdU (Fig. 1d).

To examine the extent of T_{FH} cell proliferation over time, we tracked cell division using NP-OVA-immunized mice that express mCherry-labelled histone 2b (H2B–mCh) under the control of a doxycycline (DOX)-sensitive promoter (tTA-H2B-mCh mice)[16]. The tTA-H2B-mCh mice express H2B–mCh until they are exposed to DOX, at which point the expression of H2B–mCh is suppressed, enabling the dividing cells to dilute the indicator (Fig. 1e). Exposure of NP-OVA-immunized tTA-H2B-mCh mice to DOX over three days permits the integration of T_{FH} cell division over time, as opposed to the instantaneous measurements provided by analysis of EdU incorporation or

[1]Laboratory of Molecular Immunology, The Rockefeller University, New York, NY, USA. [2]Laboratory of Lymphocyte Dynamics, The Rockefeller University, New York, NY, USA. [3]Laboratory of Mass Spectrometry and Gaseous Ion Chemistry, The Rockefeller University, New York, NY, USA. [4]Howard Hughes Medical Institute, The Rockefeller University, New York, NY, USA.
✉e-mail: jmerkensch@rockefeller.edu

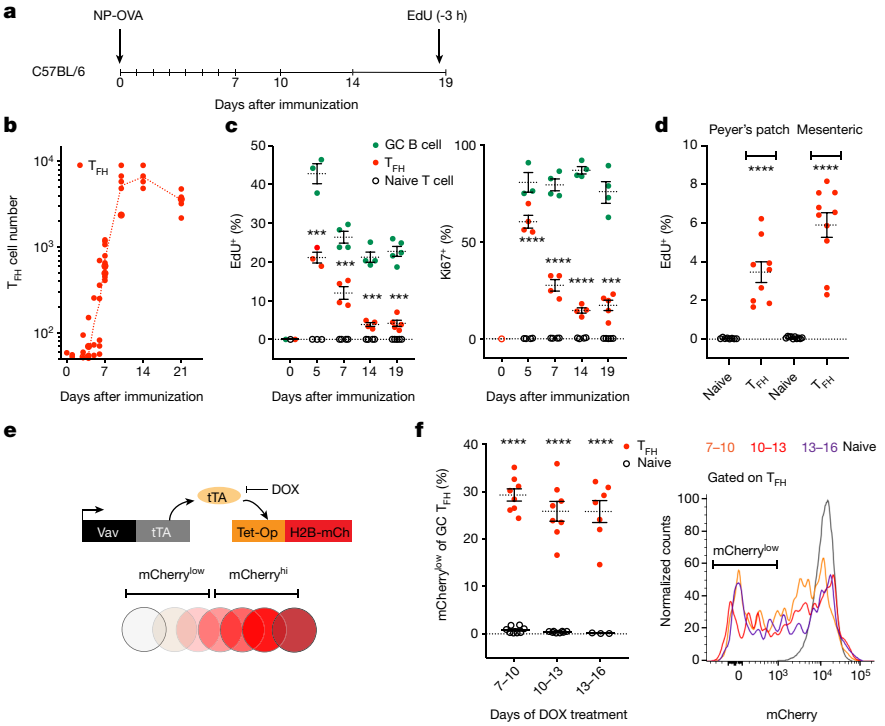

Fig. 1 | T_{FH} cells continue to divide during the GC reaction. a, Schematic representation of the experimental setup used in **b**–**d**. **b**, Kinetics of T_{FH} cell development in C57BL/6 mice after NP-OVA immunization. The absolute numbers of T_{FH} cells (red) in popliteal lymph nodes are shown. Data are from 3–5 mice per time point, each dot represents one mouse. Gating strategies are described in Extended Data Fig. 1. **c**, Plots show percentage of EdU$^+$ or Ki67$^+$ cells. Data are from 3–5 mice per time point and each dot represents one mouse. EdU was delivered 3 h before mice were culled. ***$P = 0.001$, ****$P < 0.0001$, unpaired two-tailed Student's *t*-test comparing T_{FH} and naive T cells. **d**, Plot shows percentage of EdU$^+$ cells from Peyer's patches (left) or mesenteric lymph nodes (right). Data are from 9–10 mice per group and each dot represents one mouse. ****$P < 0.0001$, unpaired two-tailed Student's *t*-test comparing T_{FH} and naive T cells. **e**, Diagrammatic representation of the Vav-tTA and Tet-Op-H2B-mCh transgenes that were combined (tTA-H2B-mCh mice) to measure cell division in the GC. **f**, Plots show frequency of naive or T_{FH} cells that became mCherry^{low} when treated with DOX between days 7 and 10 (8 mice per group), 10 and 13 (8 mice per group) or 13 and 16 (7 mice per group) after immunization with NP-OVA. Right, histogram comparing relative H2B-mCh fluorescence among T_{FH} cells during the three time windows of exposure to DOX or in naive T cells. ****$P < 0.0001$, unpaired two-tailed Student's *t*-test comparing T_{FH} and naive T cells. All experiments were performed at least twice; data are mean and s.e.m.

intranuclear Ki67 expression. On average, 27–30% of T_{FH} cells in GCs diluted H2B–mCh in response to NP-OVA when exposed to DOX on days 7–10, 10–13 or 13–16 after immunization (Fig. 1f). By contrast, we found little or no detectable division by naive T cells in the same mice.

Naive T cells proliferate extensively after activation and during their differentiation into T_{FH} cells. To ensure that the GC T_{FH} cell proliferation was not exclusively derived from newly generated T_{FH} cells, we used reporter mice that express tamoxifen-inducible Cre under the control of CD62L, which is expressed in naive T cells but not in T_{FH} cells (*Sell*-Cre^{ERT2} ROSA-tdT mice) (Extended Data Fig. 2a–c). The administration of tamoxifen to immunized *Sell*-Cre^{ERT2} ROSA-tdT reporter mice fate maps naive T cells so that they can be distinguished from contemporaneous resident T_{FH} cells if the naive cells are subsequently recruited to the GC (Extended Data Fig. 2d). Cell division was similar among recruited and resident T_{FH} in indicator mice that were injected with tamoxifen 7 days after immunization as measured by EdU labelling on day 14 (Extended Data Fig. 2e).

The proliferative kinetics of T_{FH} cells reflected the known decline in antigen availability in the days after immunization. To determine whether T_{FH} cells undergo cell division in response to antigen, we used anti-DEC205 chimeric antibodies to deliver cognate OVA protein (anti-DEC–OVA) or an irrelevant parasite protein from *Plasmodium falciparum circumsporozoite* (anti-DEC–CS) to ongoing GC reactions (through binding to DEC205 receptors on GC B cells). C57BL/6 mice were immunized with NP-OVA and boosted by the injection of anti-DEC–OVA or anti-DEC–CS[17,18] (Fig. 2a). EdU labelling 18 h after anti-DEC–OVA injection revealed antigen-dependent T_{FH} cell proliferation (Fig. 2b). Whereas 8% of T_{FH} cells were labelled with EdU at this time point in the control mice treated with anti-DEC–CS, 17% were proliferating in the mice treated with anti-DEC–OVA ($P < 0.0001$).

Naive T cells proliferate in proportion to the strength of T cell receptor (TCR) signalling. Whether persistent T_{FH} cell division is governed by the quality of TCR signalling has not been explored. Examining this in a polyclonal repertoire is challenging owing to the diversity and unknown constellation of TCR specificities that contribute to the T_{FH} cell repertoire. To examine the role of TCR signalling to T_{FH} cell proliferative responses, we used transgenic OT-II T cells that express a fixed receptor that can recognize $OVA_{323–339}$ with relatively high affinity while remaining differentially sensitive to a set of nested altered peptide ligands (APLs)[19] (Extended Data Fig. 3a). Here, the diminishing potency of each APL to elicit TCR signalling may be owing to differential loading onto MHC class II (altering the effective concentration of the ligand) or by altering TCR affinity, or both. Accordingly, OT-II T cells divide and differentiate into T_{FH} cells in direct proportion to their ability to recognize and signal in response to the corresponding APL-pMHC ligands in vitro and in vivo[20] (Extended Data Fig. 3b–f). Thus, 46% of OT-II T cells became T_{FH} cells 7 days following immunization with the high-signalling 4-hydroxyl-3-nitrophenylacetyl-APL (NP-APL) as opposed to only 12% in response to low-signalling NP-APL immunization[20] (Extended Data Fig. 3e).

To determine whether the magnitude of the TCR signalling directly affected the degree of T_{FH} cell cellular division during the GC reaction, as opposed to just pre-GC differentiation, we generated anti-DEC205–APL chimeric antibodies carrying either the high- or low-signalling APLs

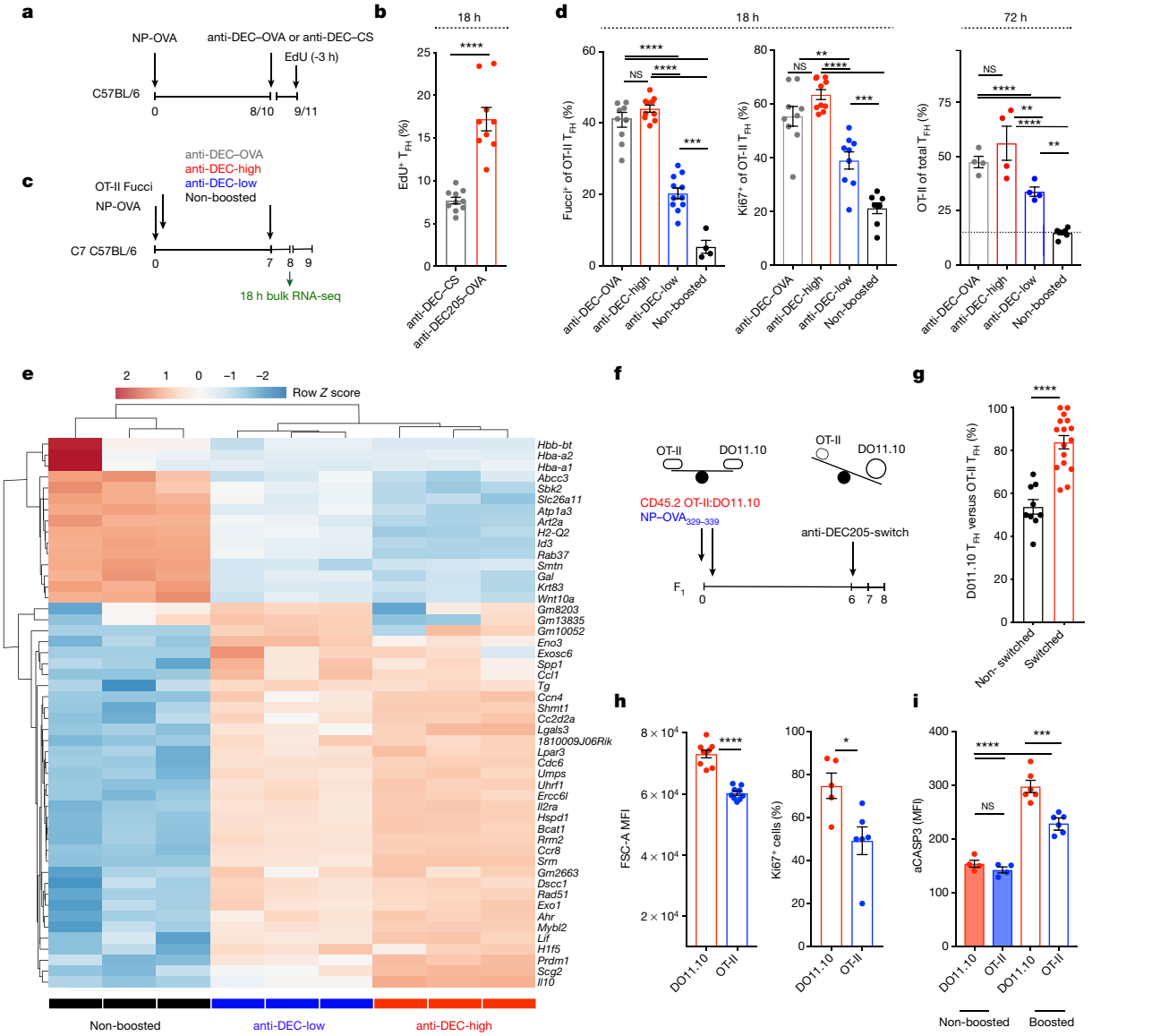

Fig. 2 | T_{FH} cells proliferate proportionately to TCR signalling. a, Schematic representation of experimental setup used in **b**. Anti-DEC-high, anti-DEC–$OVA_{323–339}$; anti-DEC-low, anti-DEC–$OVA_{329–339}$. **b**, Bar graph shows the percentage of proliferating T_{FH} cells as defined by EdU incorporation after treatment with anti-DEC–CS (10 mice) or anti-DEC–OVA (9 mice). Each dot represents an individual mouse. $P < 0.0001$ by unpaired Student's *t*-test (two-tailed). **c**, Schematic representation of experimental setup used in **d** and **e**. **d**, Left, plots showing the percentage of OT-II T_{FH} cells that express Fucci (10, 10, 10 and 4 mice per group from left to right) or Ki67 (9, 10, 9 and 8 mice per group from left to right) 18 h after injection of anti-DEC205 chimeric antibody. Each dot represents an individual mouse. $^{**}P = 0.0012$, $^{***}P = 0.0007$, $^{****}P < 0.0001$, one-way ANOVA test. Right, percentage of OT-II T cells among T_{FH} cells 72 h after injection of anti-DEC205 chimeric antibody. Data are from four mice per group and each dot represents one mouse. $^{**}P = 0.005$, $^{**}P = 0.0068$, $^{****}P < 0.0001$, one-way analysis of variance (ANOVA). **e**, Heat map of hierarchically clustered purified populations of OT-II T_{FH} cells. Comparing gene expression of the 50 most differentially expressed genes. $^{*}P = 0.0160$, $^{*}P = 0.0211$, $^{***}P < 0.001$, $^{****}P < 0.0001$, one-way ANOVA. **f**, Schematic depicting experimental setup for the competition experiment between DO11.10 and OT-II T_{FH} cells in **g**. **g**, Bar graphs compare changes in the frequency of DO11.10 versus OT-II T_{FH} cells in anti-DEC–$OVA_{323–339}$-boosted (switched) or uninjected controls (non switched). Data are from 10 or 16 mice per group and each dot represents one mouse. $^{****}P = 0.0001$, unpaired two-tailed Student's *t*-test. **h**, Bar graphs compare the size of blasting cells (left, forward scatter area (FSC-A), 8 mice per group) or the percentage of $Ki67^{+}$ cells (right, 6 or 7 mice per group) in DO11.10 or OT-II T_{FH} cell populations 18 h after exposure to anti-DEC–$OVA_{323–339}$ chimeric antibody. Each dot represents one mouse. $^{*}P = 0.0183$, $^{****}P < 0.0001$, unpaired Student's *t*-test. MFI, mean fluorescent intensity. **i**, Bar graph comparing expression of aCASP3 between non-boosted populations and in the same populations 18 h after anti-DEC–$OVA_{323–339}$ boosting. $^{***}P = 0.0001$, $^{****}P < 0.0001$, one-way ANOVA test. Each experiment was performed two or three times; data are mean and s.e.m.

(anti-DEC–$OVA_{323–339}$ or anti-DEC–$OVA_{329–339}$; hereafter anti-$DEC_{323–339}$ or anti-$DEC_{329–339}$, respectively). Cell division in response to anti-DEC–APL injection was measured using OT-II T_{FH} cells expressing a fluorescent ubiquitin-based cell cycle indicator (Fucci) that marks cells that are in the cell cycle[21,22]. OT-II Fucci naive T cells were adoptively transferred into C57BL/6 mice that were immunized with NP-OVA and then injected on day 7 with high and low anti-DEC–APLs or not injected at all and analysed 18 h later (Fig. 2c). A significantly greater number of OT-II T_{FH} cells entered the cell cycle in response to anti-DEC-high APLs than in response to anti-DEC-low APL conjugates as measured by Fucci or Ki67 staining (Fig. 2d, top right). Moreover, increased proliferation at 18 h was associated with the proportional outgrowth of OT-II T_{FH} cells compared with endogenous T_{FH} cells after 72 h (Fig. 2d, top right-most panel).

In addition to activated B cells, dendritic cells also express high levels of DEC205 receptors that could be targeted by the anti-DEC–APL

chimeric antibodies[23]. To confirm that the proliferation of T_{FH} cells was driven by cognate interactions between T_{FH} cells and GC B cells as opposed to cognate interactions between T_{FH} and DCs, we limited anti-DEC205-boosting exclusively to B cells by adoptively transferring B1-8^{+} B cells and OT-II Fucci T cells into DEC205-deficient mice (Extended Data Fig. 3g). OT-II T_{FH} cells showed significant proliferation when antigen presentation was limited to GC B cells ($P = 0.0048$) (Extended Data Fig. 3h).

Next, to verify that the proliferating cells that responded to anti-DEC205 antibody boosting were GC-resident T_{FH} cells, we used mice that carry a photoactivatable green fluorescent protein (OT-II paGFP)[24,25]. OT-II naive paGFP T cells were transferred into NP-OVA-immunized C57BL/6 mice and subsequently injected with anti-DEC–OVA on day 10 after immunization, and GC-resident T_{FH} cells were labelled by photoactivation 18 h later (Extended Data Fig. 4a–d). Flow cytometric analysis showed that 20% of GC (GFP^{+}) T_{FH} cells were in the S or G2M phases of the cell cycle (Extended Data Fig. 4e). Altogether, the data indicate that in addition to providing help, GC T_{FH} cells can undergo proliferative expansion in response to pMHC presented in the GC.

To examine the transcriptional programs that are associated with TCR-driven T_{FH} cell division, we performed mRNA sequencing (RNA-seq) on total OT-II T_{FH} cells isolated 18 h after boosting with high or low anti-DEC–APLs, and non-boosted control cells. Unsupervised hierarchical clustering segregated samples according to each condition and revealed a unique signature in the boosted OT-II T_{FH} cells (Fig. 2e). Gene set enrichment analysis (GSEA) comparing T_{FH} cells responding to high APLs versus non-boosted controls showed increased representation of pathways that regulate the cell cycle, metabolism, glycolysis and oxidative phosphorylation (Fig. 2e, Extended Data Fig. 5a). Comparison of the high and low APL groups revealed 533 differentially expressed genes, with an enrichment in cytokine and interleukin signalling in the high APL group, consistent with wider roles for TCR signalling in T_{FH} cell function (Extended Data Fig. 5b). Altogether, the data indicate that T_{FH} cells proliferate in direct proportion to their ability to recognize pMHC presented on GC B cells, and that this behaviour is sustained through a coordinated metabolic reprogramming.

High-affinity B cells outcompete their low-affinity counterparts during the GC reaction[6,16,17,26]. We next investigated whether T_{FH} cells also undergo clonal competition on the basis of their affinity for pMHC. To do so, we made use of two transgenic T cells that express $OVA_{323–339}$-specific TCRs with different affinities—DO11.10 (H2^{d}) and OT-II (H2^{b}). The DO11.10 TCR recognizes ovalbumin with approximately 50-fold higher affinity for antigen than OT-II in the context of the H2^{d} MHC haplotype[19,27,28]. To characterize relative affinities of DO11.10 and OT-II cells, which have different genetic backgrounds and so could contain distinct genes that might affect TCR signalling or responsiveness, to the APLs in the context of the MHC haplotypes H2^{b}/H2^{d} and to prevent rejection of either T cell population, we adoptively transferred them into immunized C57BL/6 × BALB/c F_1 mouse recipients (Extended Data Fig. 6a). The two cell types showed similar proliferative responses to $OVA_{329–339}$, but DO11.10 cells displayed significantly greater responses than OT-II when mice were immunized with the longer APL variants $OVA_{323–339}$, $OVA_{327–339}$ and $OVA_{328–339}$ (Extended Data Fig. 6b, c).

To determine whether T_{FH} cells continue to undergo competitive affinity-based selection once in the GC, we transferred a mixture of DO11.10 and OT-II cells into H2^{b}/H2^{d} F_1 mice and immunized them with the shorter $OVA_{329–339}$ peptide, which they recognize with relatively equal affinity, to allow both T cell types to seed GC reactions (Extended Data Fig. 6d, e). In mice that received no further intervention, the average percentage of DO11.10 T_{FH} cells was 54% and comparable to their input values (Fig. 2f, g, Extended Data Fig. 6d, e). Boosting with cognate $OVA_{329–339}$ maintained the same relative proportion of the two transgenic T cells in the GC (Extended Data Fig. 6f). By contrast, the relative representation of DO11.10 T_{FH} cells increased to 84% 48 h after

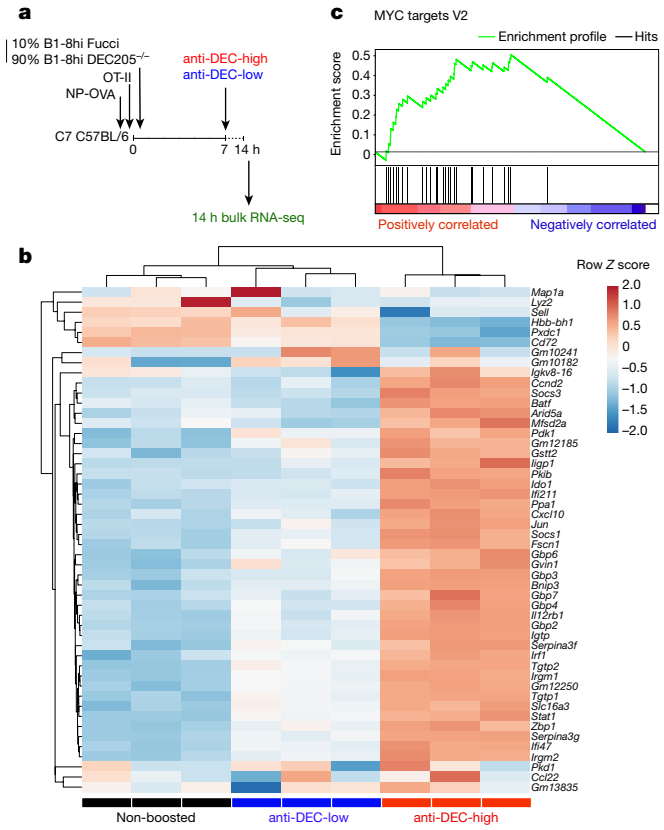

Fig. 3 | TCR signalling dictates the quality of T cell help delivered. **a**, Schematic representation of experimental setup used in **b**, **c**. The flow cytometric plots showing the gating strategy to isolate positively selected light-zone germinal centre B cells 14 h after injection of anti-DEC–APL antibody is shown in Extended Data Fig. 8. **b**, Heat map of hierarchically clustered purified populations of Fucci^{+} light-zone B cells. The expression of the 50 most differentially expressed genes is compared. **c**, Graphical representation of GSEA and the rank-ordered gene lists found upregulated in recently selected Fucci^{+} GC light-zone B cells that are boosted with anti-DEC-high versus anti-DEC-low chimeric antibodies. Nominal $P = 0.0$; enrichment score = 0.4911; normalized enrichment score (NES) = 2.64; false discovery rate (FDR) $q = 0.0$.

$OVA_{323–339}$ boosting (anti-DEC-switch) on day 6 ($P < 0.0001$; Fig. 2g, right). The outgrowth of DO11.10 T_{FH} cells, in response to boosting with an APL which increased its relative affinity compared with competitor OT-II T_{FH} cells, was driven by cell proliferation as determined by an increase in cell size and Ki67 staining despite a concomitant increase in the expression of activated caspase-3 (aCASP3) (Fig. 2h, i, Extended Data Fig. 6g). We conclude that DO11.10 and OT-II T_{FH} cells, albeit with their different genetic backgrounds withstanding, undergo competitive proliferative expansion in GCs of C57BL/6 × BALB/c F_1 recipients based on their affinities for pMHC.

The numbers of T_{FH} cells in the GC must be limiting to maintain stringent B cell selection[7,11,13–15,29,30]. Whether the quality of the T_{FH} TCR repertoire also influences the products of the GC reactions remains to be determined. To examine how signals that induce the proliferative expansion of T_{FH} cells might affect the quality of help provided to cognate B cells, we performed RNA-seq on purified, positively selected light-zone GC B cells 14 h after boosting with the anti-DEC–APLs[17,31] (Fig. 3a, b, Extended Data Fig. 7a). Unsupervised hierarchical clustering separated the mRNAs obtained from B cells responding to control (non-boosted), and high and low anti-DEC–APLs into three distinct groups (Fig. 3b). Comparison of the differentially expressed genes showed that high- APLs-boosted conditions induced higher levels of mRNAs associated with positive selection including MYC, mTORC1

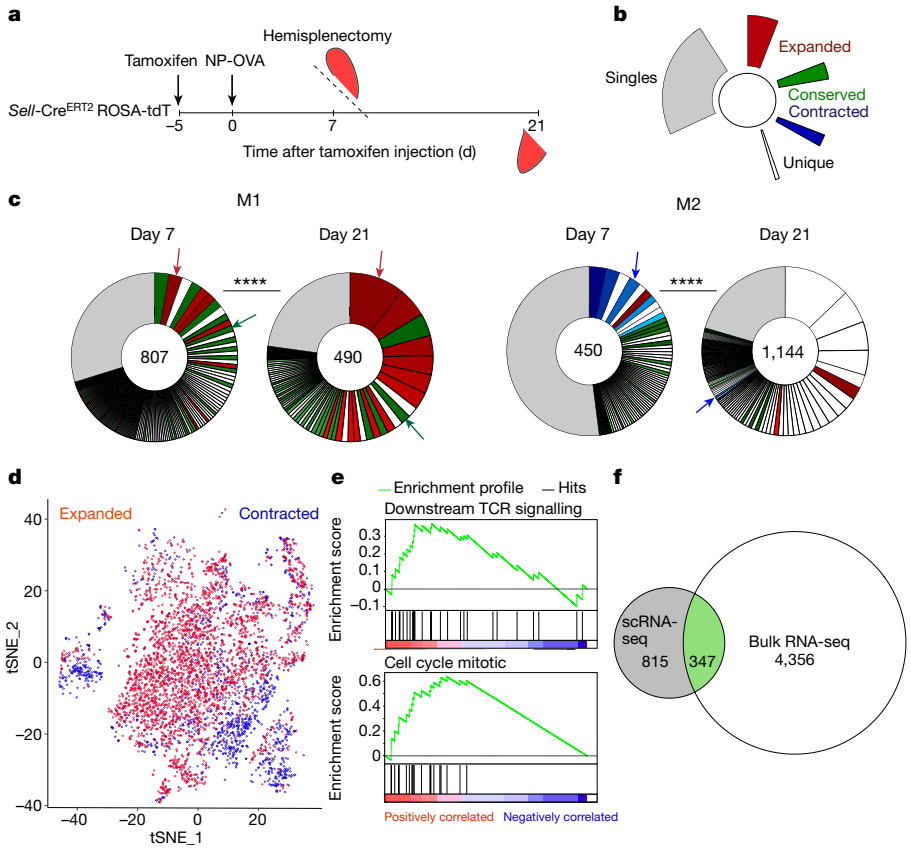

Fig. 4 | Extensive T_{FH} cell clonal evolution. a, Schematic representation of experimental setup. **b**, Colour coded indexing for the clonal behaviours between days 7 and 21. Clones that appear white were unique to each time point, either contracting or expanding between the time points. **c**, Pie charts show clonal populations of T_{FH} cells within each mouse (M) at each time point. Segments within the pie charts report the proportional representation of each clone. Clonotypes contain the same CDR3 sequence for the alpha or/and beta chains. ****$P < 0.0001$, Fisher exact test. Red, green or blue arrows denote examples of clones found between time point that expanded, contracted or were relatively conserved, respectively. Numbers inside the pie charts refer to the total number of TCR sequences. **d**, *t*-distributed stochastic neighbour embedding (*t*-SNE) plot calculated using 20 principal component analysis (PCA) dimensions on single-cell RNA sequencing (scRNA-seq) data, comparing transcriptome of all expanded clones versus all contracted clones (pooled between all mice). **e**, GSEA of differentially expressed genes between clones that expanded or contracted. Downstream TCR signalling: nominal $P = 0.0029$; enrichment score = 0.37; NES = 1.84; FDR $q = 0.036$. Regulation of mitotic cell cycle: nominal $P = 0.00$; enrichment score = 0.63; NES = 2.71; FDR $q = 0.00$. **f**, Euler diagram comparing the number of shared genes between the scRNA-seq (grey) and OT-II bulk RNA-seq (white) that have the same behaviour, either up or downregulated (green).

and cell division pathways than the non-boosted or low-APL-boosted conditions[31] (Fig. 3c, Extended Data Fig. 7b). Thus, the ability of the T cells to recognize cognate pMHC governs their ability to divide, the extent of trophic cytokine production and the magnitude of the selection signals provided to GC B cells.

Unlike GC B cells, T_{FH} cells distribute among nascent GCs in lymph nodes and continue to emigrate between GCs during the immune response[1]. To determine whether 'polyclonal' T_{FH} cell clones also disseminate throughout GCs in the spleen, we compared their distribution in the two halves of spleens obtained 7 days after NP-OVA immunization (Extended Data Fig. 8a, b). As expected, T_{FH} cell clones were shared and their relative distribution was similar between the two halves of the spleen as determined by TCR-α and TCR-β sequencing (Extended Data Fig. 8c).

To determine whether there is dynamic redistribution of T_{FH} cell clones during a polyclonal immune response, we followed T_{FH} cell clonotypes in the same mouse longitudinally by performing hemi-splenectomy on day 7 and then collecting the remaining half of the spleen on day 21 after immunization with NP-OVA, a procedure that did not measurably alter the size of the GC compartment per se (Fig. 4a, Extended Data Fig. 9a, b). To ensure that we assayed T cells entering spleen GCs de novo during the immunization period, we used *Sell*-CreERT2 ROSA-tdT mice (Extended Data Figs. 2, 9d, e). Naive cells were labelled in reporter mice 5 days before immunization and T_{FH} cells responding to the immunization were purified from hemi-splenectomized mice on days 7 and 21 based on tdTomato expression (Fig. 4a, Extended Data Fig. 10a). Single-cell RNA-seq (scRNA-seq) revealed a significant ($P < 0.001$) dynamic re-distribution of T_{FH} cell clones between the two time points in all six mice analysed (Fig. 4b, c, Extended Data Fig. 10b–d). TCR-α and TCR-β sequencing showed that 55% and 73% of all T_{FH} cells were members of expanded clones on days 7 and 21, respectively. A total of 86% of the day 7 clones expanded or contracted between days 7 and 21, and only 13% were relatively conserved (examples noted by red, blue and green arrows in Fig. 4c).

To determine whether there are gene expression signatures associated with T_{FH} cell clonal expansion or contraction, we analysed the transcriptome of single cells belonging to clones exhibiting these behaviours. Cells belonging to clones that expand or contract were segregated by principle component analysis (Fig. 4d). In agreement with the RNA-seq data obtained from OT-II T_{FH} cells (Fig. 2e), gene set enrichment analysis (GSEA) revealed that the mRNAs expressed by clones that expand after day 7 differed from those that contracted, were genes expressed that are involved in TCR signalling and cell division (Fig. 4e). In addition, 347 of the 815 differentially expressed genes

between the clones that expanded or contracted after day 7 did so in parallel to the genes that were up- or downregulated within OT-II T_{FH} cells in response to increased antigen presentation in the GC (Figs. 2e, 4f). We conclude that clones of T_{FH} cells undergo considerable dynamic changes in response to antigen during polyclonal immune responses in the germinal centre.

The GC reaction is governed by T_{FH} cells that select high-affinity B cells that present the highest levels of pMHC[24]. Although T cells cannot mutate their receptors and must remain limiting to maintain stringent B cell selection, our data indicate that ongoing T cell selection shapes T_{FH} cell repertoires during the immune response[32].

Limiting numbers of T_{FH} cells govern selection in the GC[2,33–35]. A paucity of T_{FH} cells results in diminished antibody responses to viral infections in mice and macaques[13–15]. By contrast, overabundance of T_{FH} cells interferes with affinity maturation and is associated with auto-immunity[11,30]. To maintain homeostasis, T_{FH} cells are thought to limit their own proliferative responses to TCR stimulation by high-level expression of negative regulators such as PD1, SLAMF6 and LAG-3[12,29]. Nevertheless, T_{FH} cells remain sufficiently responsive to pMHC to provide help to cognate B cells in the form of trophic cytokines. Our data indicate that in addition to triggering T cell help, interaction between T_{FH} cells and cognate pMHCII on GC B cells also favours affinity-based selection of T_{FH} cells in the GC.

Selection of T_{FH} cells with increased sensitivity to pMHC across GCs during the reaction is likely to prolong the immune response in the face of ever decreasing amounts of antigen. In addition, enhanced TCR signalling by affinity-selected T_{FH} cells may account for increased production of plasma cells in the later stages of the GC reaction[36]. In conclusion, the clonal dynamics that govern the relationship between GC B cells and T_{FH} cells is even more dynamic and symbiotic than previously envisaged.

Online content

Any methods, additional references, Nature Research reporting summaries, source data, extended data, supplementary information, acknowledgements, peer review information; details of author contributions and competing interests; and statements of data and code availability are available at https://doi.org/10.1038/s41586-021-03187-x.

1. Shulman, Z. et al. T follicular helper cell dynamics in germinal centers. *Science* **341**, 673–677 (2013).
2. Schwickert, T. A. et al. A dynamic T cell-limited checkpoint regulates affinity-dependent B cell entry into the germinal center. *J. Exp. Med.* **208**, 1243–1252 (2011).
3. Crotty, S. T follicular helper cell biology: a decade of discovery and diseases. *Immunity* **50**, 1132–1148 (2019).
4. Vinuesa, C. G., Linterman, M. A., Yu, D. & MacLennan, I. C. M. Follicular helper T cells. *Annu. Rev. Immunol.* **34**, 335–368 (2016).
5. Cyster, J. G. & Allen, C. D. C. B cell responses: cell interaction dynamics and decisions. *Cell* **177**, 524–540 (2019).
6. Victora, G. D. & Nussenzweig, M. C. Germinal centers. *Annu. Rev. Immunol.* **30**, 429–457 (2012).
7. Pratama, A. & Vinuesa, C. G. Control of TFH cell numbers: why and how? *Immunol. Cell Biol.* **92**, 40–48 (2014).
8. Shulman, Z. et al. Dynamic signaling by T follicular helper cells during germinal center B cell selection. *Science* **345**, 1058–1062 (2014).
9. Kitano, M. et al. Bcl6 protein expression shapes pre-germinal center B cell dynamics and follicular helper T cell heterogeneity. *Immunity* **34**, 961–972 (2011).
10. Crotty, S. Follicular helper CD4 T cells (TFH). *Annu. Rev. Immunol.* **29**, 621–663 (2011).
11. Linterman, M. A. et al. Follicular helper T cells are required for systemic autoimmunity. *J. Exp. Med.* **206**, 561–576 (2009).
12. Cubas, R. A. et al. Inadequate T follicular cell help impairs B cell immunity during HIV infection. *Nat. Med.* **19**, 494–499 (2013).
13. Harker, J. A., Lewis, G. M., Mack, L. & Zuniga, E. I. Late interleukin-6 escalates T follicular helper cell responses and controls a chronic viral infection. *Science* **334**, 825–829 (2011).
14. Fahey, L. M. et al. Viral persistence redirects CD4 T cell differentiation toward T follicular helper cells. *J. Exp. Med.* **208**, 987–999 (2011).
15. Locci, M. et al. Human circulating PD-1^{+}CXCR3^{-}CXCR5^{+} memory Tfh cells are highly functional and correlate with broadly neutralizing HIV antibody responses. *Immunity* **39**, 758–769 (2013).
16. Gitlin, A. D., Shulman, Z. & Nussenzweig, M. C. Clonal selection in the germinal centre by regulated proliferation and hypermutation. *Nature* **509**, 637–640 (2014).
17. Gitlin, A. D. et al. T cell help controls the speed of the cell cycle in germinal center B cells. *Science* **349**, 643–646 (2015).
18. Hawiger, D. et al. Dendritic cells induce peripheral T cell unresponsiveness under steady state conditions in vivo. *J. Exp. Med.* **194**, 769–779 (2001).
19. Robertson, J. M., Jensen, P. E. & Evavold, B. D. DO11.10 and OT-II T cells recognize a C-terminal ovalbumin 323-339 epitope. *J. Immunol.* **164**, 4706–4712 (2000).
20. Tubo, N. J. et al. Single naive CD4^{+} T cells from a diverse repertoire produce different effector cell types during infection. *Cell* **153**, 785–796 (2013).
21. Sakaue-Sawano, A. et al. Visualizing spatiotemporal dynamics of multicellular cell-cycle progression. *Cell* **132**, 487–498 (2008).
22. Aiba, Y. et al. Preferential localization of IgG memory B cells adjacent to contracted germinal centers. *Proc. Natl Acad. Sci. USA* **107**, 12192–12197 (2010).
23. Jiang, W. et al. The receptor DEC-205 expressed by dendritic cells and thymic epithelial cells is involved in antigen processing. *Nature* **375**, 151–155 (1995).
24. Victora, G. D. et al. Germinal center dynamics revealed by multiphoton microscopy with a photoactivatable fluorescent reporter. *Cell* **143**, 592–605 (2010).
25. Patterson, G. H. & Lippincott-Schwartz, J. A photoactivatable GFP for selective photolabeling of proteins and cells. *Science* **297**, 1873–1877 (2002).
26. Lau, A. W. & Brink, R. Selection in the germinal center. *Curr. Opin. Immunol.* **63**, 29–34 (2020).
27. Barnden, M. J., Allison, J., Heath, W. R. & Carbone, F. R. Defective TCR expression in transgenic mice constructed using cDNA-based alpha- and beta-chain genes under the control of heterologous regulatory elements. *Immunol. Cell Biol.* **76**, 34–40 (1998).
28. Hu, J., Qi, Q. & August, A. Itk derived signals regulate the expression of Th-POK and controls the development of CD4 T cells. *PLoS ONE* **5**, e8891 (2010).
29. Crotty, S. T follicular helper cell differentiation, function, and roles in disease. *Immunity* **41**, 529–542 (2014).
30. Vinuesa, C. G., Tangye, S. G., Moser, B. & Mackay, C. R. Follicular B helper T cells in antibody responses and autoimmunity. *Nat. Rev. Immunol.* **5**, 853–865 (2005).
31. Finkin, S., Hartweger, H., Oliveira, T. Y., Kara, E. E. & Nussenzweig, M. C. Protein amounts of the MYC transcription factor determine germinal center B cell division capacity. *Immunity* **51**, 324–336.e5 (2019).
32. Merkenschlager, J. et al. Stepwise B-cell-dependent expansion of T helper clonotypes diversifies the T-cell response. *Nat. Commun.* **7**, 10281 (2016).
33. de Vinuesa, C. G. et al. Germinal centers without T cells. *J. Exp. Med.* **191**, 485–494 (2000).
34. Johnston, R. J. et al. Bcl6 and Blimp-1 are reciprocal and antagonistic regulators of T follicular helper cell differentiation. *Science* **325**, 1006–1010 (2009).
35. Rolf, J. et al. Phosphoinositide 3-kinase activity in T cells regulates the magnitude of the germinal center reaction. *J. Immunol.* **185**, 4042–4052 (2010).
36. Weisel, F. J., Zuccarino-Catania, G. V., Chikina, M. & Shlomchik, M. J. A Temporal switch in the germinal center determines differential output of memory B and plasma cells. *Immunity* **44**, 116–130 (2016).

Methods

Mice

Mice were housed at a temperature of 72 °F (22 °C) and humidity of 30–70% in a 12-h light/dark cycle with ad libitum access to food and water. Male and female mice aged 8–10 weeks at the start of the experiment were used throughout. C57BL/6J, BALB/c, OT-II (C57BL/6J) and DO11.10 (BALB/c) mice were purchased from Jackson Laboratories. Fucci transgenic mice were obtained from T. Kurosaki and A. Miyawaki. C7 mice were obtained from the S. Rudensky laboratory. OT-II Fucci, tTa-H2B-mCh mice, OT-II paGFP and *DEC205*$^{-/-}$ (also known as *Ly75*^{tm1Mnz}) mice were generated and maintained at Rockefeller University. *Sell*-CreERT2 ROSA-tdT reporter mice were generated in CY2.4 albino B6 embryonic stem (ES) cells and exclusively crossed to B6 animals for 10 generations and maintained at Rockefeller University. C57BL/6 × BALB/c F_1 mice were bred to be used as recipients of OT-II (C57BL/6J) and DO11.10 (BALB/c) CD4 T cells in competition experiments. It should be noted that transferred OT-II (C57BL/6J) and DO11.10 (BALB/c) remained on their original genetic background and so might have a range of intrinsic differences that could not be fully controlled for in these experiments. All mouse experiments were performed under Institutional Review Board approved protocols. Sample sizes were not calculated a priori. Given the nature of the comparisons, mice were not randomized into each experimental group and investigators were not blinded to group allocation.

Immunizations and treatments

C57BL/6J, *Sell*-CreERT2 ROSA-tdT, C7, tTa-H2B-mCh mice or F_1 recipient mice (6–12 weeks old) were immunized with 20 μg or 50 μg of NP17–OVA (Biosearch Technologies) precipitated in alum in footpads or intraperitoneally respectively. For NP-APL immunizations, 100 μM of each hapten was precipitated in alum at a 2:1 ratio and injected into footpads.

Anti-DEC–OVA, anti-DEC–CS and anti-DEC–APL chimeric antibodies were transiently expressed in 293-6E cells using polyethylenimine (PEI, Sigma 408727) for transfection. The supernatant was collected 7 days later and the chimeric antibodies were concentrated by ammonium sulfate precipitation. After centrifugation the pellet was resuspended in PBS and affinity purified on Protein G columns (Protein G Sepharose 4 Fast Flow, 17-0618-05, GE Healthcare).

Two micrograms of chimeric antibody in PBS was injected into footpads of the recipient mice at indicated time points. Deletion of *loxP*-flanked alleles was induced by intraperitoneal injection of tamoxifen (Sigma) dissolved in corn oil (Sigma) at indicated doses (10 mg per mouse) and time points. For tTA-H2B-mCherry dilution experiments, mice were administered DOX (doxycycline hyclate, Sigma) by intraperitoneal injection of 2 mg DOX in PBS and footpad injection of 0.2m g DOX in PBS. Mice were maintained on DOX by adding DOX (2 mg ml^{-1}) and sucrose (50 mg ml^{-1}) to the drinking water for the indicated time periods. Draining lymph nodes were collected for flow cytometric analysis. H2B–mCh dilution was monitored by flow cytometry.

Hemi-splenectomy

Mice were kept on antibiotics prior to immunization as prophylaxis against infection after surgical intervention. On day 7 after immunization, mice were anaesthetized with isoflurane. The left side of the mouse was shaved and cleaned before an incision was made in the skin followed by a smaller incision in the peritoneal wall to allow access to the spleen. The section of spleen to be removed was tied off by using sutures to prevent bleeding, and then cut out while leaving the splenic artery intact. The peritoneal wall was closed and stitched using perma-hand silk 5-0 sutures (Ethicon). The skin was closed using 9 mm wound clips (Clay Adams brand, Becton Dickinson). After recovery from anaesthesia, mice were transferred to a new clean cage with a heating pad.

T cell transfer and culture

Single-cell suspensions were prepared from the spleens and lymph nodes of donor mice. CD4$^+$ T cells were enriched using immunomagnetic negative selection (StemCell Technologies). For adoptive transfer experiments 0.5×10^6–1×10^6 CD4$^+$ T cells were injected into recipient mice by intravenous injection.

Peptide synthesis

The peptides were created using a Protein Technologies Symphony peptide synthesizer on pre-coupled Fmoc-Lysine(e-biotinyl)-OH Wang resins (Bachem). Reactions were conducted at a 100-μM scale and elongated using 9-fluorenylmethoxycarbonyl (Fmoc)-protected amino acids. Deprotection of the amine was accomplished with 20% piperidine in NMP (*N*-methylpyrrolidinone). Repetitive coupling reactions were conducted using 0.3 M HATU in Cl$^-$HOBT and 0.6 M DIEA using NMP as the primary solvent.

The peptides were capped at amine terminus with a 4-hydroxy-3-nitrophenyl acetic acid label. Resin cleavage and side-chain deprotection was achieved by transferring beads to a 100 ml round bottom flask which are then reacted (room temperature in fume hood) with 8.0 ml concentrated, sequencing grade, trifluoroacetic acid including a scavenger mixture of triisopropylsilane and degassed water, in a ratio of 94:3:3 over 6 h. Column filtration removed the resin, dispensing it into a 50-ml round bottom flask. The TFA/peptide solution volume was then reduced to 2 ml through these of a rotary evaporator. A standard ether precipitation was conducted on the peptides by transferring the solution to a 50 ml falcon tube containing 40 ml of cold TBME (tert-butyl methyl ether). Tube was then placed in an ice bath for 2 h to aid in precipitation, followed by pellet formation using centrifugation (3,300 rpm for 5 min). Excess ether was removed by vacuum aspiration and the peptide pellet was then allowed to dry overnight in a fume hood. Peptide was then dissolved in 20% acetonitrile and 10 ml HPLC grade water, subsampled for liquid chromatography–mass spectrometry (LC–MS) and lyophilized. This crude product was analysed by reversed-phase Aquity UPLC using a Waters BEH C18 column and monitoring 220 nm absorbance. Peptide integrity was simultaneously verified by a capillary split flow into a tandem electrospray mass spectrometer using a ThermoFinnigan LTQ system. Preparative chromatography purification was accomplished on a Vydac C18 RP preparative column on a Waters 600 Prep HPLC. Fractions are collected in 30 s intervals, with each characterized using LC–MS on the above system and the fractions containing desired product are then lyophilized, weighed and provided to Nussenzweig laboratory.

B cell transfer

Single-cell suspensions were prepared from the spleens and lymph nodes of donor mice. Resting B cell suspensions were enriched using immunomagnetic positive selection using CD43 (StemCell Technologies). Approximately 5×10^6 B1-8$^+$ B cells (5×10^5 Igλ$^+$, NP-specific B cells) composed of the indicated populations were injected into recipient mice by intravenous injection.

T cell activation in vitro

Peritoneal macrophages or B cells were collected and plated in flat bottomed 96-well plates as a source of antigen-presenting cells. On the next day, CD4+ T cells were enriched from spleens by magnetic bead selection (StemCell Technologies) and labelled with CTV. Approximately 100,000 CTV-labelled or unlabelled cells were then co-cultured with the antigen-presenting cells and the indicated amount of the APLs and T cell activation was assessed 18 h later by flow cytometry.

T cell activation in vivo

CD4$^+$ T cells were enriched from spleens by magnetic bead selection (StemCell Technologies) and labelled with CTV. CTV labelled cells were then injected into mice and the quality of the T-cell response assessed 3–7 days later by flow cytometry.

Flow cytometry

Single-cell suspensions were stained with antibodies directly conjugated to surface markers. Intracellular stains were performed using

commercially available Fix and permeabilization solutions coupled to incubation with ki67, aCASP3 or DAPI antibodies. Multi-colour cytometry was performed on the Symphony flow cytometer (BD biosciences) and analysed with FlowJo v10.4.2.

Photoactivation

To label light-zone-resident follicular dendritic cells, 10 µl of 1 mg ml^{-1} of B-phycoerthrin (Invitrogen) was mixed with 1 µl of 10 mg ml^{-1} rabbit anti-PE (Thermo) and injected into pre-immunized mice, 2 days before imaging. Lymph nodes were collected and then cleared of adipose tissue under a dissecting microscope and placed in PBS between two coverslips held together by vacuum grease. FDC networks were identified by imaging at l = 950 nm, at which no photoactivation is observed, and 3D regions of interest were photoactivated by higher-power scanning at l = 830 nm. Imaging experiments were performed using an Olympus FV1000 upright microscope fitted with a 25× 1.05 NA Plan water-immersion objective and a Mai-Tai DeepSee Ti-Sapphire laser (Spectraphysics).

RNA sequencing

For bulk RNA-seq experiments, congenic OT-II T_{FH} cells (CD4$^+$, CD62^{low}, CXCR5^{hi}, PD-1^{hi}) or positively selected B cells (500 cells) were purified by flow cytometry 18 h after pre-immunized host mice were injected with anti-DEC205 chimeric antibodies. One nanogram of total RNA was used to generate full-length cDNA using Clontech's SMART-Seq v4 Ultra Low Input RNA Kit (634888). The cDNA was used to prepare libraries using Illumina Nextera XT DNA sample preparation kit (FC-131-1024). Libraries with unique barcodes were pooled at equal molar ratios and sequenced on an Illumina NextSeq 500 sequencer to produce 75-bp reads, following manufacture protocol (15048776).

For scRNA-seq, single-cell suspensions were prepared from half-spleens of NP-OVA immunized *Sell*-CreERT2 ROSA-tdT mice on days 7 and 21 after immunization. Samples were indexed with TotalSeqC (BioLegend) cell surface antibodies and CD4$^+$, CD62^{low}, CD44^{hi}, PD1^{hi}, CXCR5^{high}, tdTomato$^+$ T_{FH} cells were purified by flow cytometry, pooled and loaded onto a Chromium Controller (10x Genomics). Single-cell RNA-seq libraries were prepared using the Chromium Single Cell 5′ v2 Reagent Kit (10x Genomics) according to manufacturer's protocol. Libraries were loaded onto an Illumina NextSeq with the mid-Output Kit (150 paired end) for V-D-J analysis or NOVAseq for single-cell gene expression. Hashtag indexing was used to demultiplex the sequencing data and generate gene-barcode matrices, respectively.

Statistical analyses

Statistical tests were conducted using Prism (GraphPad) software. Unpaired, two-tailed Student's t-tests and one-way ANOVA with Tukey's post hoc tests to further examine pairwise differences were used. Data were considered statistically significant at $^*P \le 0.05$, $^{**}P \le 0.01$, $^{***}P \le 0.001$, and $^{****}P \le 0.0001$. The number of mice per group, number of replicates and the nature of error bars are indicated in the legend of each figure. Centre bars always indicate mean and error bars denote s.e.m.

Computational analysis

For differential gene expression analysis in the bulk RNA-seq experiments we used kallisto (v.0.46) to map sequence reads to *Mus musculus* transcriptome (GRCm38/ Ensembl release 99). Kallisto TPM values were converted to absolute counts using tximport (v.1.12.3) R package and DESeq2 (v.1.24.0) was used for differential expression analysis. Differentially expressed genes were defined by having an adjusted $P < 0.05$ and $|\log FC| > \log_2(1.5)$. In the Venn diagrams common differentially expressed genes also had common behaviour between groups, that is, up and down between the two data sets. Hierarchical clustering was based on combined data from three experimental repeats. Hierarchical clustering done based on data from the individual repeats gave similar results.

For single-cell RNA-seq analysis we used Cell Ranger (v.3.0.2) 10x Genomics for single-cell UMI quantification and TCR clonotype assembly. Hashtag-oligos (HTOs) UMI counts were processed using CITE-Seq-Count (v.1.4.0). We used Seurat (v.3.1.2), an R package to analyse single cell RNA-seq data, to identify differentially expressed genes. Genes expressed in at least 10% of all cells belonging to clones exhibiting expansion or contraction, with the adjusted P value by Bonferroni correction less than 0.05 and with $|\text{average } \log_e FC| > \log_e(1.1)$ were selected as statistically significant differentially expressed genes.

To define T_{FH} cell clonal behaviours, we used multiple binomial tests to interrogate whether the frequency of cells of a specific clone in the second time point is greater or less than expected, according to the frequency of the same clone in the first time point. Adjusted P values (q value) were calculated using the FDR correction. Expanded clones were defined as having cell frequency greater than expected in the second time point ($q < 0.05$), while contracted clones were defined as having cell frequency less than expected in the second time point ($q < 0.05$). Clones without statistical significance for any test were classified as conserved clones.

Ethical statement

All procedures in mice were performed in accordance to protocols approved by the Rockefeller University IACUC. All animal experiments were performed according to the protocols approved by the Institutional Animal Care and Use Commitee of NIAID, NIH.

Antibodies

Lists of monoclonal antibodies produced and their characteristics are in Supplementary Table 1.

Reporting summary

Further information on research design is available in the Nature Research Reporting Summary linked to this paper.

Data availability

The data discussed in this publication have been deposited in the NCBI Gene Expression Omnibus are accessible through GEO series accession number GSE147182.

Acknowledgements We thank A. Miyawaki and T. Kurosaki for the Fucci mice, E. E. Kara and T. Hagglof for the generation and maintenance of *Sell*-CreERT2 ROSA-tdT reporter mice, H. Zebroski for the generation of the APLs and the NP-APL conjugates in house, T. Eisenreich for help with mouse colony management, and technical help, A. Escolano for advice, B. Zhang and C. Zhao at The Rockefeller University Genomics Resource Center for assistance with 10x genomics and high-throughput sequencing, K. Gordon and K. Chhosphel for assistance with cell sorting, and all members of the Nussenzweig laboratory for discussions. We thank G. Victora for discussions involving the photoactivation experiments. This work was supported by National Institutes of Health (NIH) grant 5R37 AI037526 and NIH Center for HIV/AIDS Vaccine Immunology and Immunogen Discovery (CHAVID) 1UM1AI144462-01 to M.C.N. J.M. is an EMBO fellow. M.C.N. is an HHMI investigator.

Author contributions J.M., S.F. and M.C.N. conceived, designed and analysed the experiments. J.M., S.F. and J.K. carried out all experiments. A.G. and M.C. produced anti-DEC205-conjugates. C.R.N. contributed to paGFP experiments and discussions. H.H. bred and helped generate the *Sell*-CreERT2 ROSA-tdT mice. V.R. and T.Y.O. performed the bioinformatic analysis. B.T.C., W.Z. and P.D.B.O. helped perform the characterization on APL MHC class II occupancy. J.M. and M.C.N. wrote the manuscript with input from all co-authors.

Competing interests The authors declare no competing interests.

Additional information
Supplementary information The online version contains supplementary material available at https://doi.org/10.1038/s41586-021-03187-x.
Correspondence and requests for materials should be addressed to J.M.
Peer review information *Nature* thanks the anonymous, reviewer(s) for their contribution to the peer review of this work.
Reprints and permissions information is available at http://www.nature.com/reprints.

a

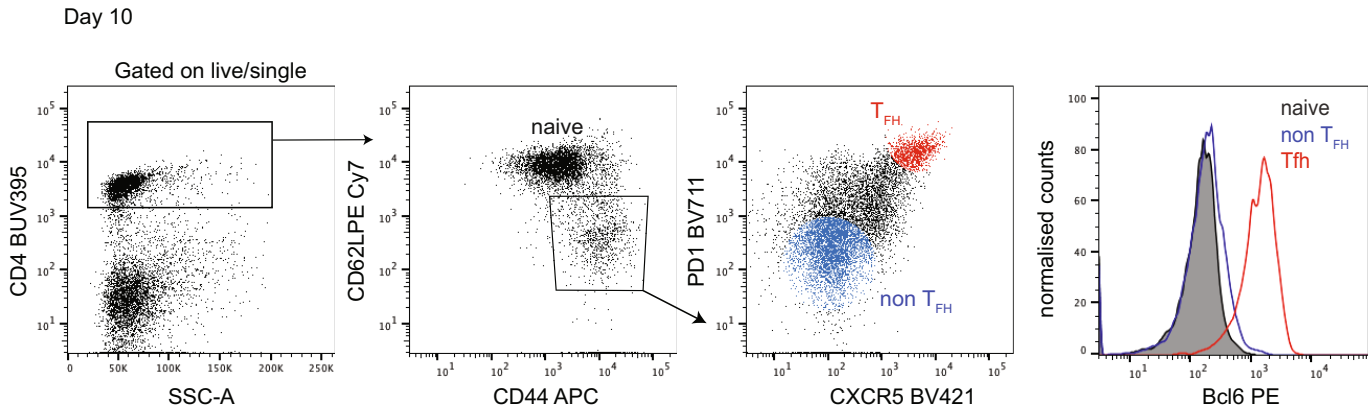

Extended Data Fig. 1 | T_{FH} cell gating strategy. a, Flow cytometry plots detailing the T_{FH} cell gating strategy. Rightmost histogram compares BCL6 expression in naive (grey) and non T_{FH} (blue) versus T_{FH} (red) cell populations on day 10 after immunization.

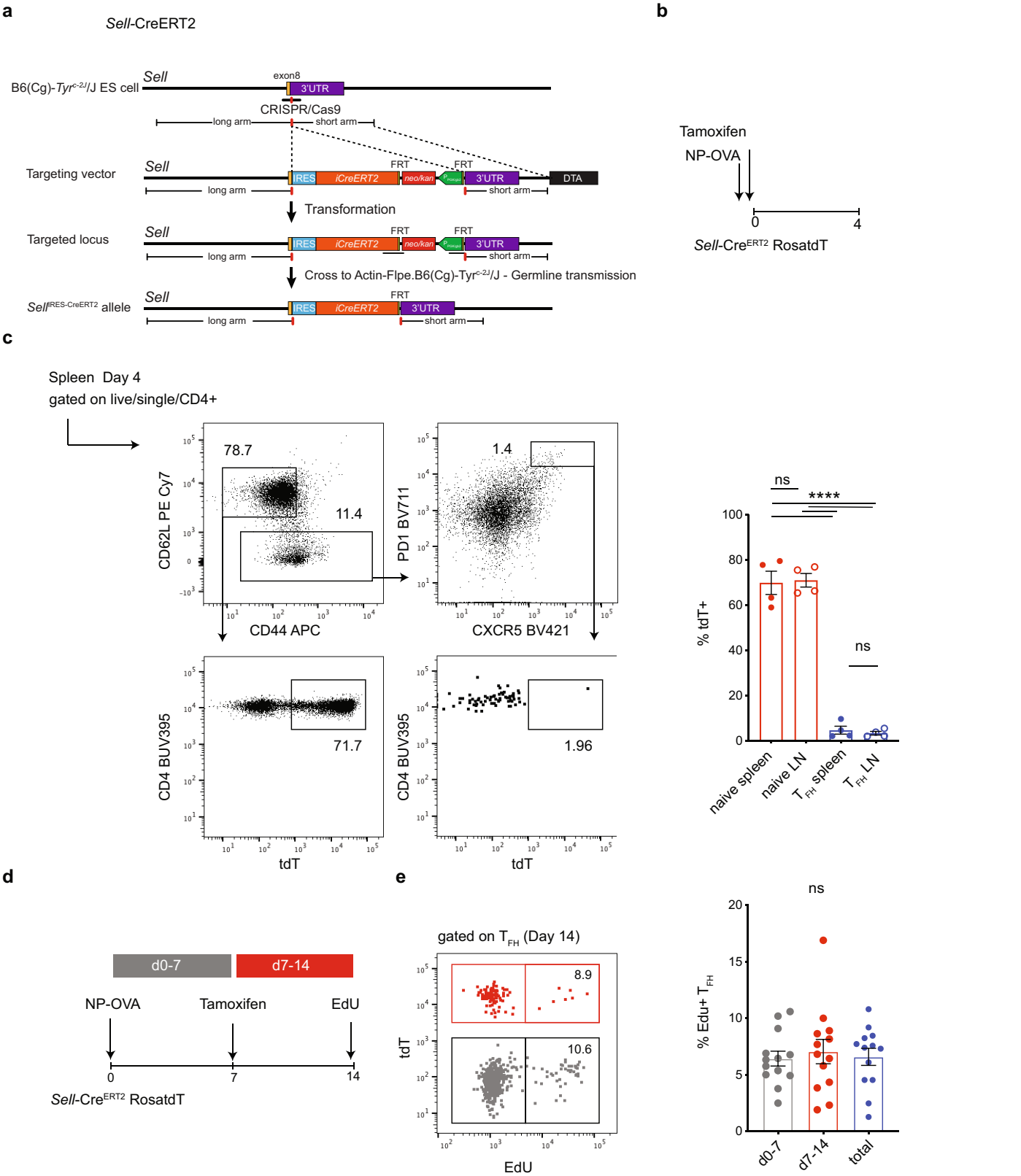

Extended Data Fig. 2 | Production of *Sell*-Cre^{ERT2} ROSA-tdT indicator mice. **a**, Targeting strategy and the configuration of the *Sell*$^{fRES\text{-}CreERT2}$ allele. The mice were produced at Rockefeller University and crossed to ROSA tdTomato$^{loxP/loxP}$ to generate *Sell*-Cre^{ERT2} ROSA-tdT indicator mice. **b**, Schematic representation of the experimental strategy used in **c**. **c**, Flow cytometry plots profiling tdTomato expression in naive and T_{FH} cell splenic compartments in tamoxifen treated mice culled 4 dpi. Rightmost plots compare the percentage of tdTomato labelling in naive T cells (red) and T_{FH} cells (blue) residing in spleens (closed circle) or lymph nodes (open circle) of mice following the regime outlined in **b**. Data are from 4–5 mice per group and each dot represents one mouse. $^{****}P < 0.0001$, one-way ANOVA test. The experiment was performed twice. **d**, Schematic representation of the experimental setup. **e**, Flow cytometry plot showing EdU incorporation in labelled (red) or unlabelled (grey) T_{FH} cell populations on 14 dpi. Rightmost plot shows the frequency of EdU positive T_{FH} cells at 14 dpi, in population generated in the first 7 days (grey) or 8 and 14 from day 7 onwards (red) or the cumulative (blue). EdU was administered 3 h before mice were culled. Numbers inside the gates denote the relative representation of EdU$^+$ cells from within tdTomato$^+$ or tdTomato$^-$ populations. Each dot represents one mouse. Data are from 14 mice and the experiment was performed twice.

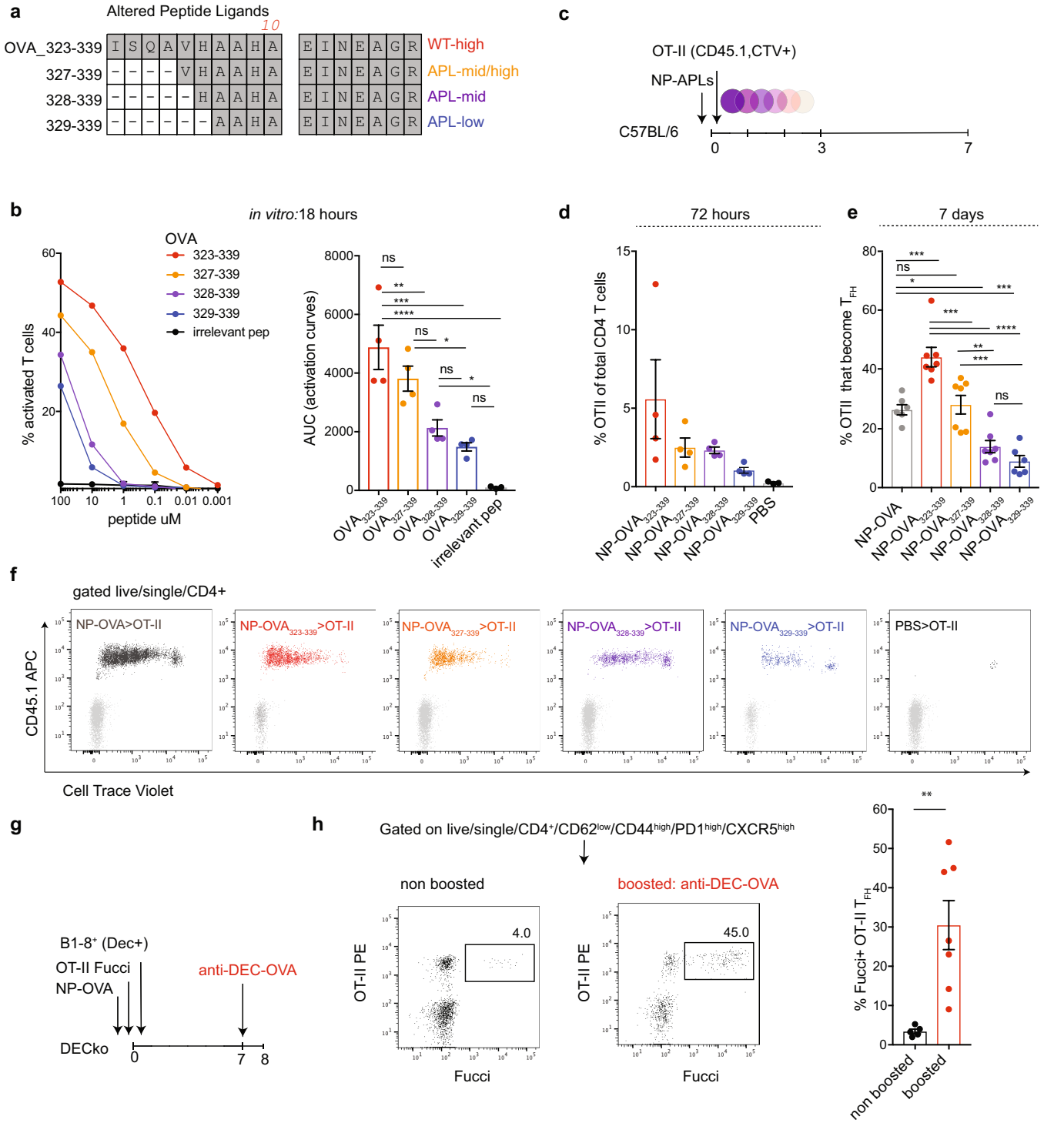

Extended Data Fig. 3 | OT-II have disparate abilities to recognize the truncated APLs. a, Description and sequence alignment of the nested APLs. **b**, Graph shows OT-II T cell responses to decreasing concentrations of APLs in vitro as measured by CD69 upregulation after 18 h of exposure. Bar graph shows the area under the adjacent response curves (AUC). $^{*}P = 0.0130$, $^{***}P = 0.0001$, $^{****}P < 0.0001$, one-way ANOVA test. Each dot represents a distinct experimental well. This experiment was repeated four times. **c**, Schematic representation of experimental setup used in **d**–**f**. **d**, Bar graph shows percentage of OT-II among all CD4 T cells in adoptive transfer recipients 72 h after immunization with the indicated NP-APLs. **e**, Bar graph shows percentage of OT-II T cells that become T_{FH} cells 7 days after NP-APL immunization. $^{*}P = 0.0186$, $^{**}P = 0.0039$, $^{***}P < 0.001$, $^{****}P < 0.0001$, one-way ANOVA test. Each dot represents one mouse, with 6 or 7 mice per group and repeated twice. **f**, Flow cytometry plots showing dilution of CellTrace Violet by OT-II T cells responding to the NP-APL immunization in vivo after 72 h. Each plot is an individual mouse. **g**, Schematic representation of experimental setup used in **h**. **h**, Left, flow cytometry plots profiling Fucci expression in non-boosted (5 mice) control or 18 h after anti-DEC–OVA (7 mice) injection. Right, comparison of the percentage of Fucci^{+} OT-II T_{FH} cells in the respective conditions. Each dot represents a mouse and this experiment was performed twice. $^{**}P = 0.0048$, unpaired Student's *t*-test.

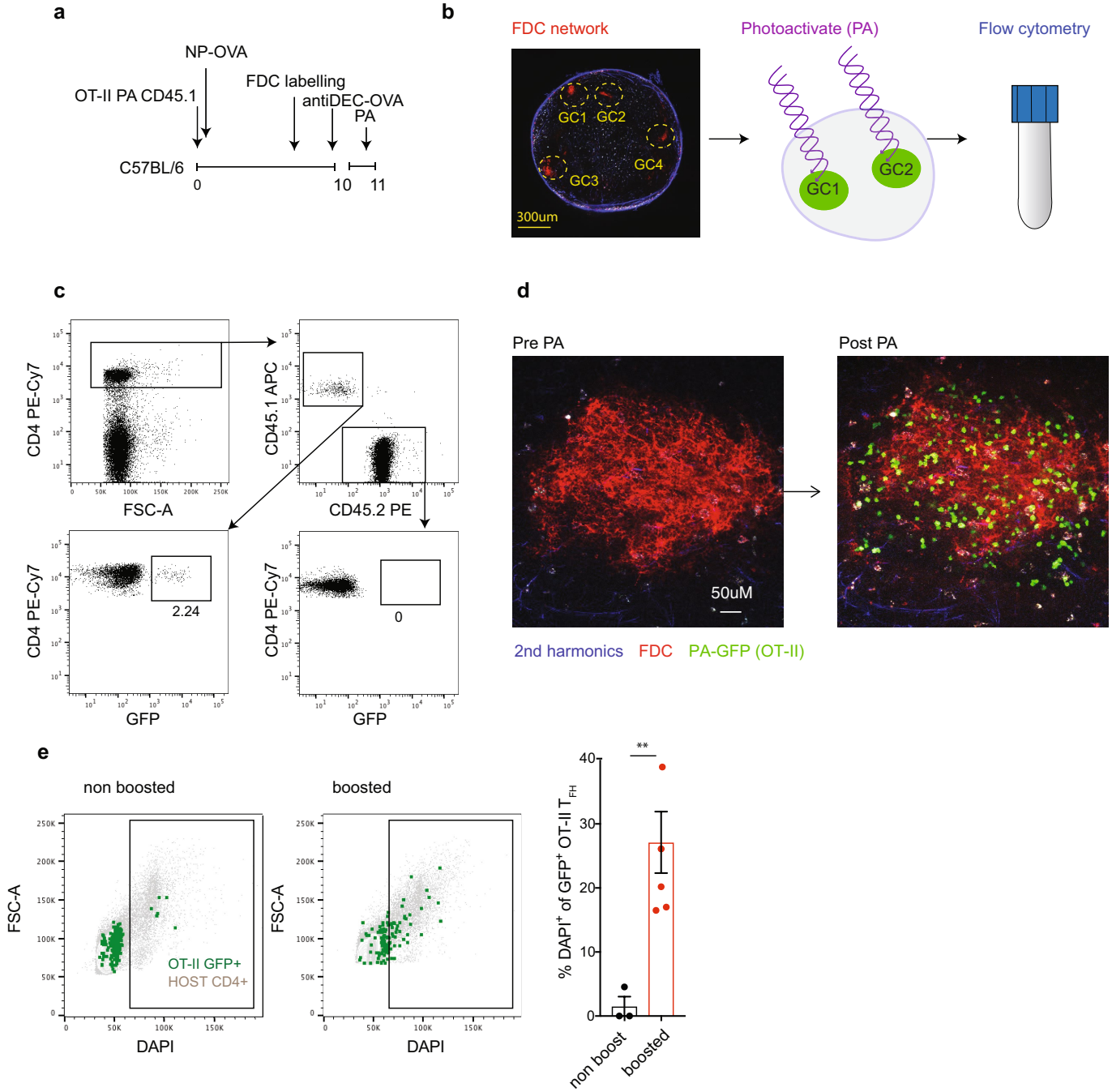

Extended Data Fig. 4 | GC-resident T_{FH} cells proliferate. a, Schematic representation of experimental set up used in **b**–**e**. **b**, GCs in popliteal lymph nodes, as defined by the fluorescently labelled FDC network (red), were photoactivated (green) 18 h after anti-DEC–OVA injection, stained with a cocktail of fluorescent antibodies to allow analysis by downstream flow cytometry. **c**, Representative flow cytometry plots showing the gating of photoactivated OT-II T_{FH} cells. **d**, A single GC from a popliteal lymph node as defined by fluorescently labelled FDC networks (red) before and after photoactivation (left to right, respectively). OT-II GC resident T_{FH} cells were photoactivated (green) 18 h after anti-DEC–OVA injection. **e**, Representative flow cytometry plots comparing DAPI staining in host (grey) or OT-II GC-resident GFP^+ cells (green) in unperturbed mice (left) or 18 h after boosting with an anti-DEC–OVA injection (right). Bar graph shows the percentage of photoactivated OT-II T_{FH} cells that entered the cell cycle ($DAPI^+$) after anti-DEC–OVA injection (5 mice) or in uninjected controls (3 mice). Each dot represents pooled lymph nodes from a single mouse. $^{**}P = 0.0086$, unpaired Student's *t*-test. This experiment was repeated twice.

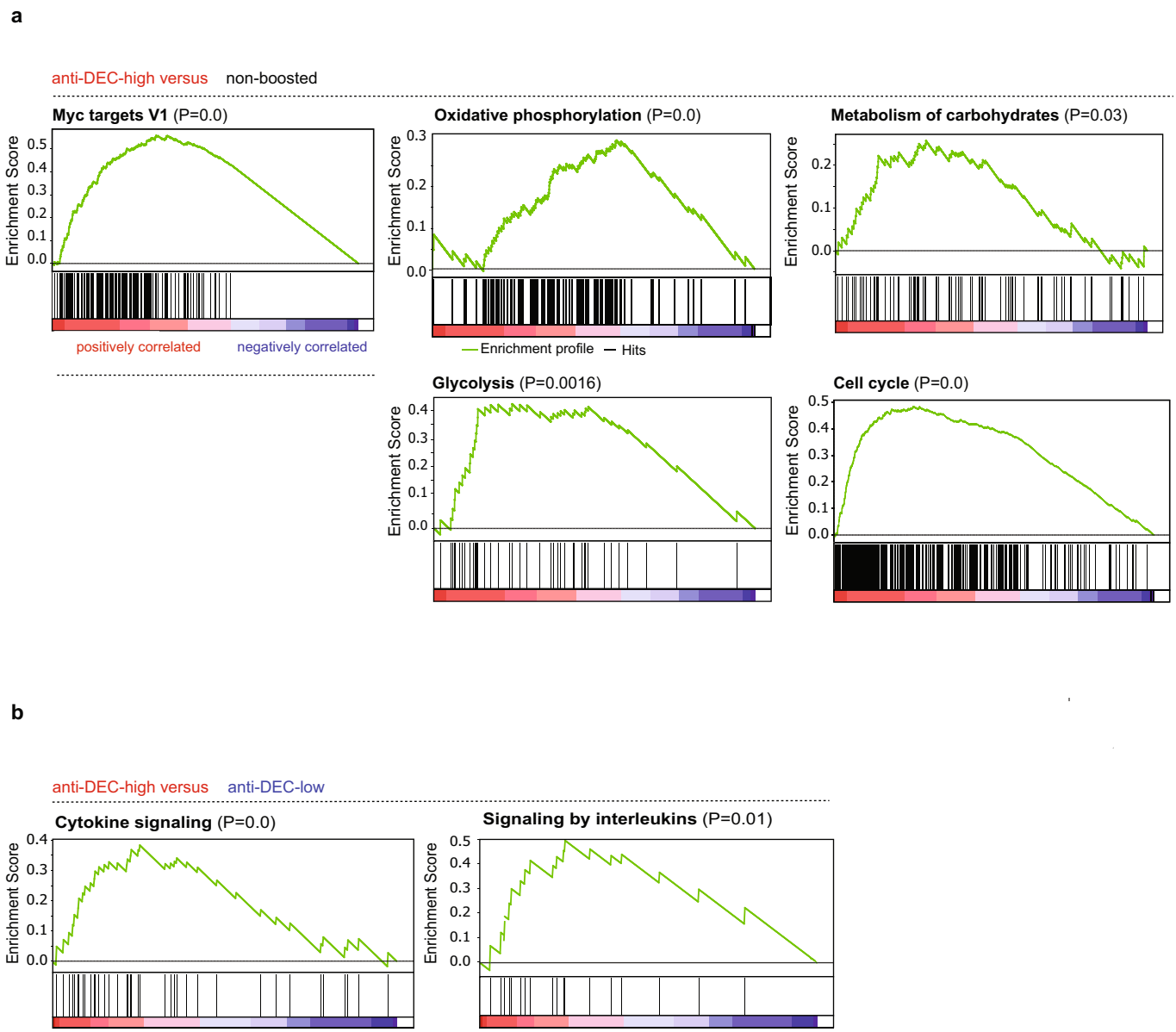

Extended Data Fig. 5 | Increased TCR signalling enforces proliferation supported by a switch in metabolic status. a, **b**, GSEA and the rank-ordered gene lists found upregulated in anti-DEC-high versus non-boosted (**a**) or anti-DEC-high versus anti-DEC-low (**b**) groups. Nominal *P* values are indicated.

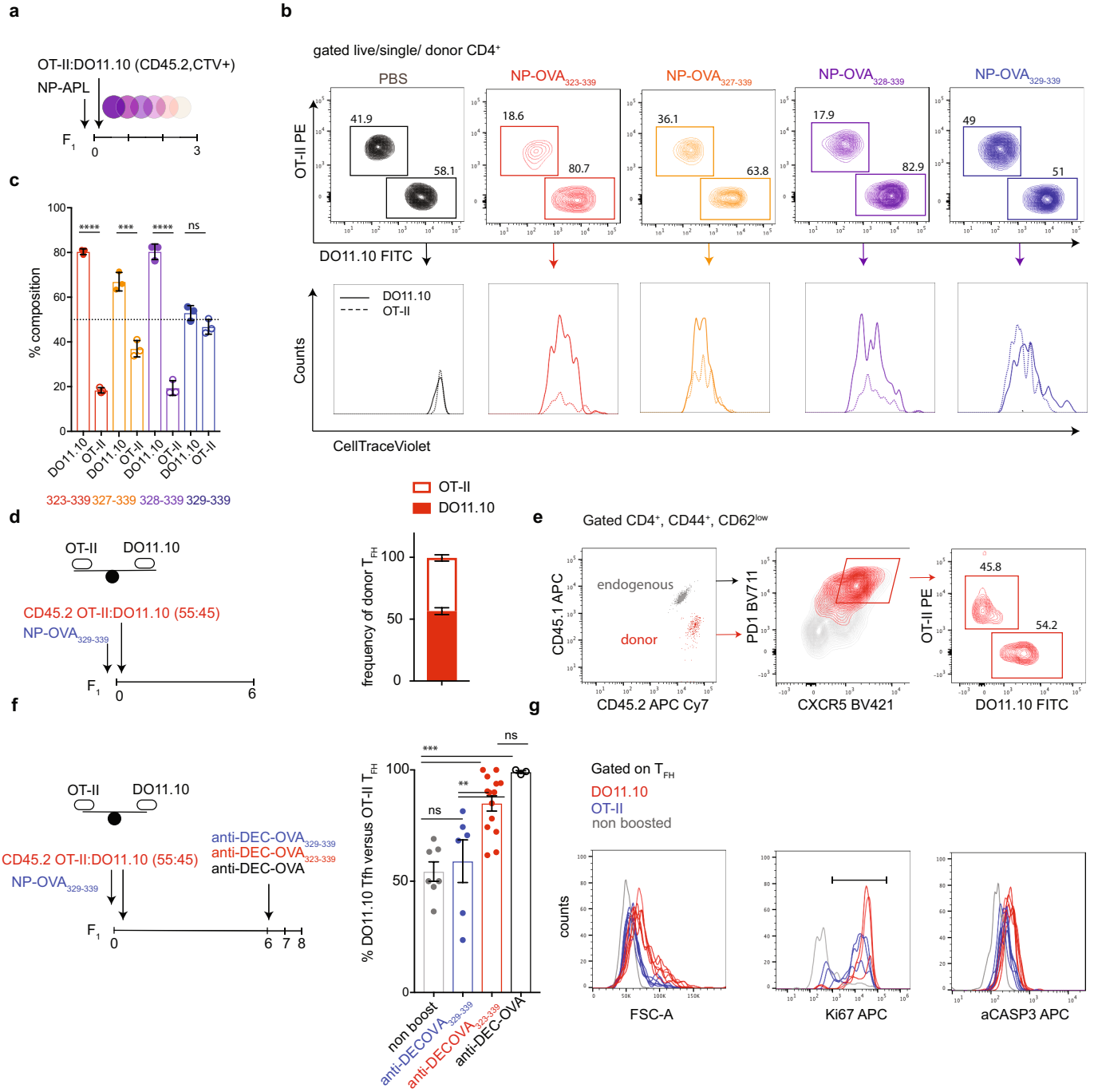

Extended Data Fig. 6 | DO11 and OT-II have different affinities for APLs. **a**, Schematic depicts the experimental setup. CTV-labelled DO11.10 and OT-II T cells were adoptively transferred into F_1 mice and subsequently immunized with the NP-APLs. **b**, Representative flow cytometry plots compare the relative distribution and CellTrace Violet dilution of DO11.10 and OT-II T cells in adoptive transfer recipients at 3 dpi. Each panel of plots represents an individual mouse from the group. **c**, Bar graph shows the aggregate relative contribution of DO11.10 and OT-II T cells 3 days after immunization in 3 mice per condition. Dotted line depicts the input ratio of DO11.10 and OT-II at the time of transfer. ***$P = 0.0007$, ****$P < 0.0001$, unpaired Student's t-test. This experiment was performed twice but data for one experiment are plotted. **d**, Schematic depicting experiment in which adoptive transfer recipients of DO11.10 and OT-II T cells were immunized with NP-329-339. Adjacent bar graph shows the aggregate relative contribution of DO11.10 and OT-II T cells 6 days after immunization with NP-$OVA_{329-339}$. **e**, Representative flow cytometry plots showing the distribution of DO11.10 and OT-II T cells in the T_{FH} cell compartment 6 days after immunization. **f**, Schematic depicting experiment in which adoptive transfer recipients of DO11.10 and OT-II T cells were immunized with NP-329-339 and boosted with the respective anti-DEC205 chimeric antibodies. Bar graph compares changes in the frequency of DO11.10 versus OT-II T_{FH} cells when boosted with different anti-DEC205 chimeric antibodies at 6 dpi. Each dot represents an individual mouse and group size varied from 3–13 mice per condition. ns, not significant ($P = 0.9$). **$P < 0.01$, ***$P < 0.001$, one-way ANOVA test. **g**, Histogram overlays compare cell size (FSC-A), Ki67 expression and aCASP3 expression in OT-II and DO11.10 T_{FH} cell populations from individual mice 18 h after anti-DEC–$OVA_{323-339}$ boosting. These experiments were repeated two or three times.

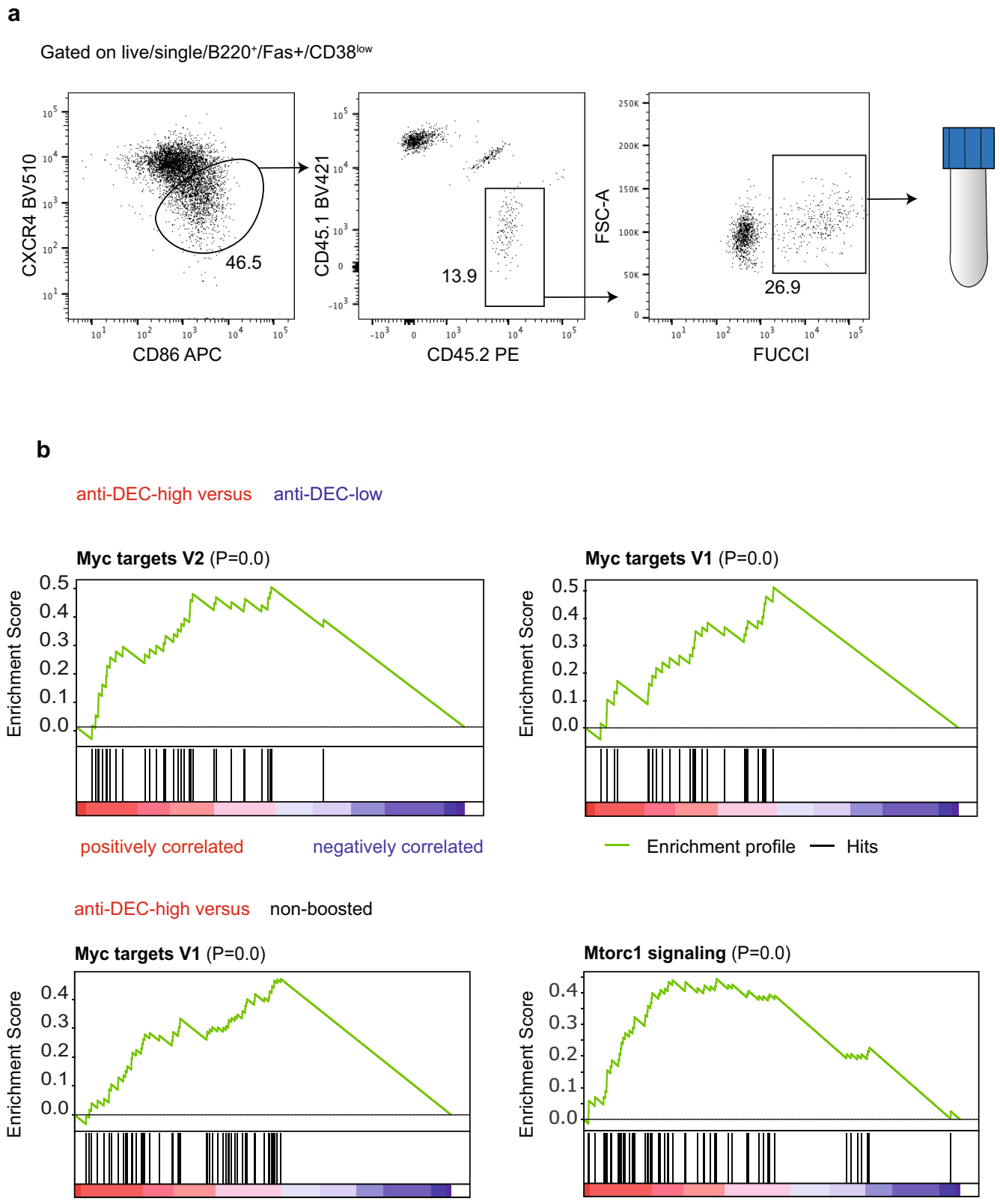

Extended Data Fig. 7 | TCR signalling dictates the quality of T cell help delivered to cognate B cells. a, Flow cytometric plots showing the gating strategy to isolate positively selected light-zone germinal centre B cells 14 h after anti-DEC–APL antibody injection. **b**, Top, graphical representation of GSEA and the rank-ordered gene lists found upregulated in anti-DEC-high versus anti-DEC-low boosted and recently selected Fucci$^+$ GC light-zone B cells. Bottom, graphical representation of GSEA and the rank-ordered gene lists found upregulated in anti-DEC-high boosted versus non-boosted controls. Nominal *P* values are indicated.

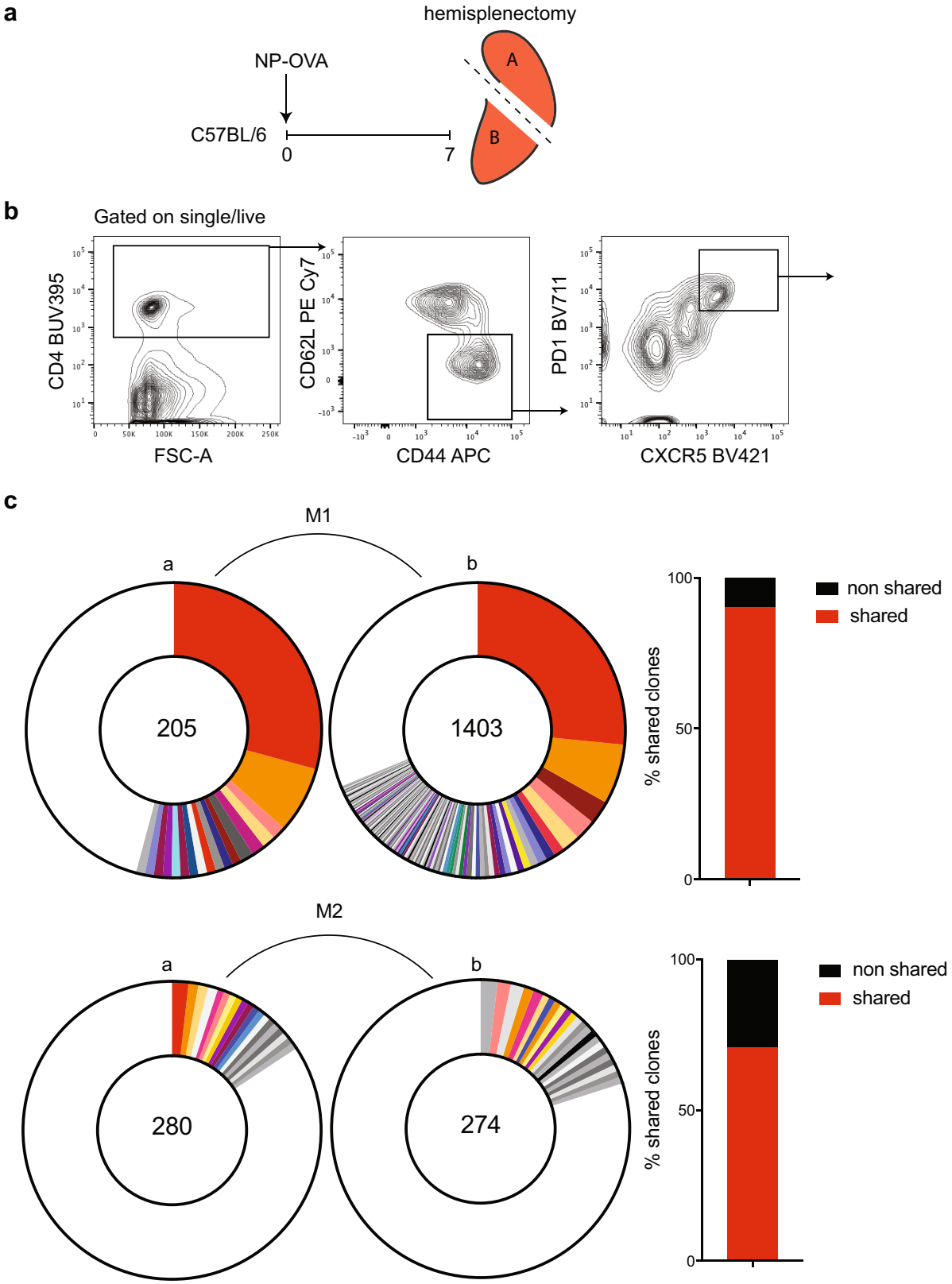

Extended Data Fig. 8 | Conservation of T_{FH} cell clonal families and clonal dominance in the spleens of day-7 immunized mice. a, Schematic representation of the experimental strategy used in **b**, **c**. **b**, Flow cytometric plots depict the gating strategy used to define T_{FH} cell populations in **c**. In brief, wild-type mice were immunized with NP-OVA, and 7 days later T_{FH} cells were purified from the two halves of the spleen and then sequenced. **c**, Pie charts show expanded clonal families in each half of the spleen. Slices are proportional to the number of clones within a family. Colours indicate shared clonotypes (cells that share the same CDR3 sequence for alpha or/and beta chains) between the two spleen halves, 'a' and 'b', from an individual mouse. Grey tones indicate unique clones not shared between the two halves. The total number of paired TCR chains recovered is indicated by the number in the centre of the pie charts. Clonal distribution between adjacent spleen halves in mouse 1 (M1) (top) (not significant, $P = 0.2279$) and mouse 2 (M2) (bottom, $P = 0.009$), Fisher's exact test. Adjacent bar graphs show the relative conservation of clonotypes between the two halves of the spleen. 'Shared' refers to a clone found in both segments of the spleen; 'non-shared' refers to anatomically novel clones.

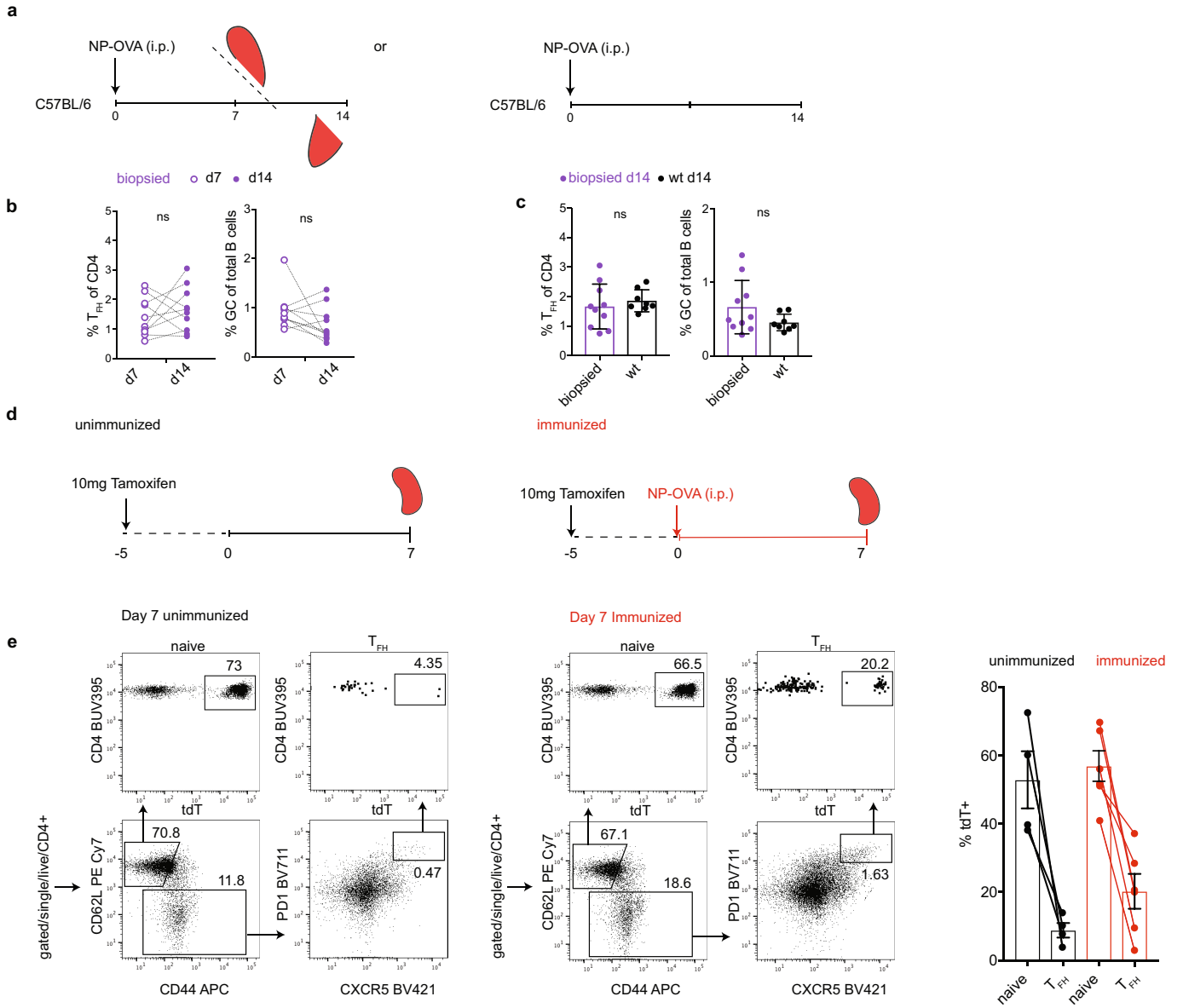

Extended Data Fig. 9 | Hemi-splenectomized mice have normal GC reactions. a, Schematic representation of the experimental strategy used in **b**, **c**. In brief, NP-OVA-immunized C57BL/6 mice were biopsied on 7 dpi and culled on 14 dpi to interrogate changes that might occur in the GC compartment after surgical intervention (left). NP-OVA-immunized C57BL/6 mice who did not receive surgical intervention served as controls for biopsied mice (right). **b**, Adjacent plots show the frequency of T_{FH} cells within total $CD4^+$ T cells (left) or GC B cells within total B cells (right) in individual biopsied mice between time points 7 dpi (open purple) and 14 dpi (closed purple). $P = 0.43$ (left) and $P = 0.14$ (right), paired Student's *t*-test. Dotted lines trace individual mice over time. **c**, Adjacent plots compare the frequency of T_{FH} cells within total CD4 T cells (left) or GC B cells within total B cells (right) at 14 dpi in mice that were biopsied (purple) or C57BL/6 mice that were not (black). $P = 0.52$ (left), $P = 0.13$ (right), Student's *t*-test. **d**, Schematic representation of the experimental strategy used in **e**. **e**, Flow cytometry plots profiling of tdTomato expression in splenic naive and T_{FH} cell compartments in tamoxifen-treated mice but unimmunized mice (left) or similarly in tamoxifen treated mice 7 days after NP-OVA immunization (right). Rightmost bar graph compares the percentage of $tdTomato^+$ populations between labelled populations in the unimmunized and immunized mice (12 days after tamoxifen administration and 7 dpi).

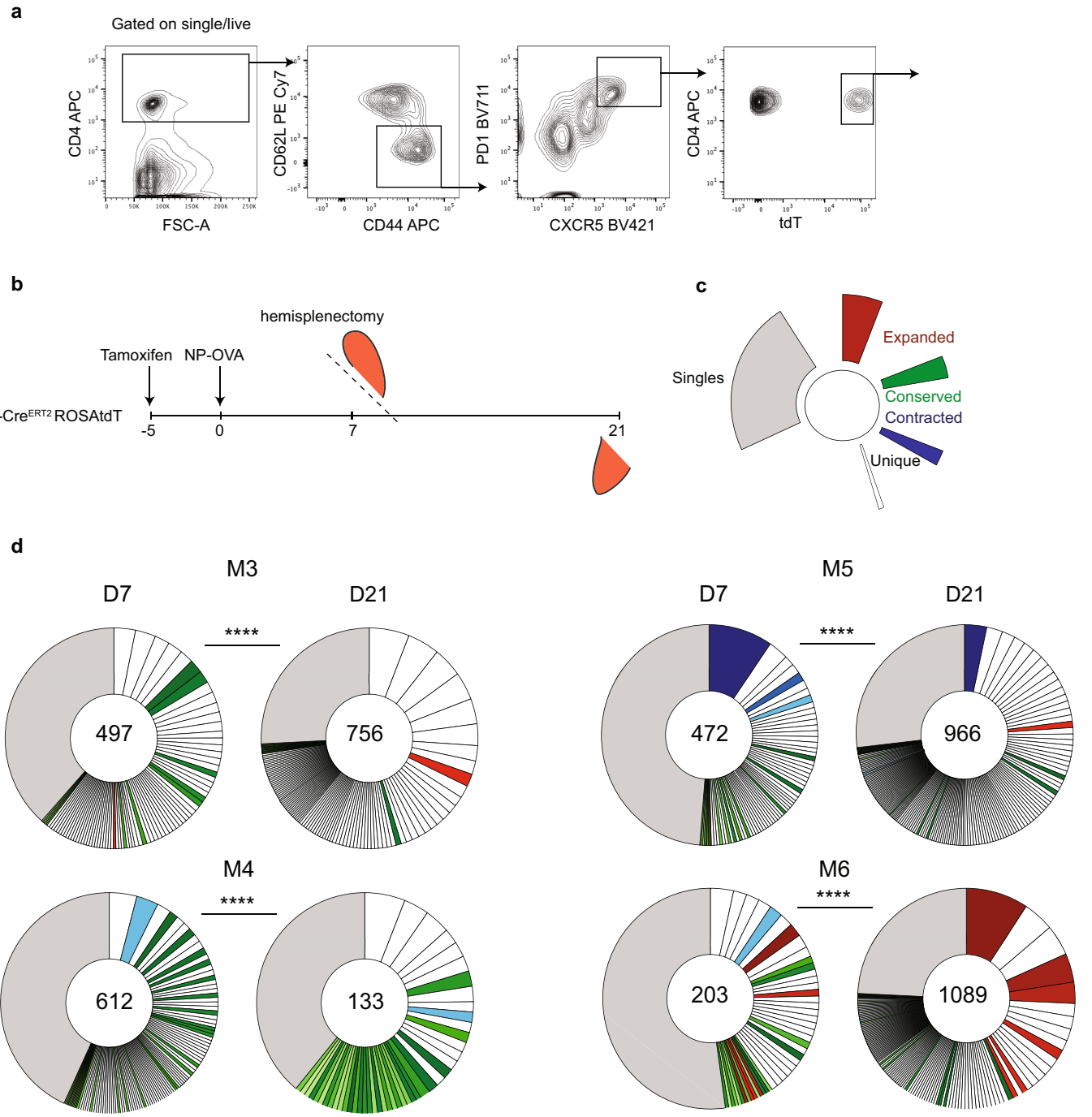

Extended Data Fig. 10 | scRNA-seq reveals extensive clonal evolution of T_{FH} cells. a, Flow cytometry plots depicting gating strategy used to define responding T_{FH} cells. **b**, Schematic representation of the experimental strategy used in **d**. **c**, Colour-coded indexing for the clonal behaviours categorized in mice between days 7 and 21. Expanded (red), conserved (green), contracted (blue) and singles (grey). Clones that are not coloured were novel to each time point. **d**, Pie charts show clonal populations of T_{FH} cells within each mouse at each time point. Segments within the pie charts report the proportional representation of each clone. Clonotypes contain the same CDR3 sequence for alpha or/and beta chains. Clonal composition is significantly different between time points within the same mouse. ****$P = 0.000016$, Fisher exact test. Numbers inside the pie charts refer to the total number of TCR-α and TCR-β sequences recovered.

nature research

Corresponding author(s): Michel Nussenzweig

Last updated by author(s): Nov 30, 2020

Reporting Summary

Nature Research wishes to improve the reproducibility of the work that we publish. This form provides structure for consistency and transparency in reporting. For further information on Nature Research policies, see Authors & Referees and the Editorial Policy Checklist.

Statistics

For all statistical analyses, confirm that the following items are present in the figure legend, table legend, main text, or Methods section.

n/a	Confirmed
☐	☒ The exact sample size (*n*) for each experimental group/condition, given as a discrete number and unit of measurement
☐	☒ A statement on whether measurements were taken from distinct samples or whether the same sample was measured repeatedly
☐	☒ The statistical test(s) used AND whether they are one- or two-sided *Only common tests should be described solely by name; describe more complex techniques in the Methods section.*
☐	☒ A description of all covariates tested
☐	☒ A description of any assumptions or corrections, such as tests of normality and adjustment for multiple comparisons
☐	☒ A full description of the statistical parameters including central tendency (e.g. means) or other basic estimates (e.g. regression coefficient) AND variation (e.g. standard deviation) or associated estimates of uncertainty (e.g. confidence intervals)
☐	☒ For null hypothesis testing, the test statistic (e.g. *F*, *t*, *r*) with confidence intervals, effect sizes, degrees of freedom and *P* value noted *Give P values as exact values whenever suitable.*
☒	☐ For Bayesian analysis, information on the choice of priors and Markov chain Monte Carlo settings
☐	☒ For hierarchical and complex designs, identification of the appropriate level for tests and full reporting of outcomes
☒	☐ Estimates of effect sizes (e.g. Cohen's *d*, Pearson's *r*), indicating how they were calculated

Our web collection on statistics for biologists contains articles on many of the points above.

Software and code

Policy information about availability of computer code

Data collection	Flow cytometry data was collected using FACDIVA version 8.0.2.
Data analysis	MacVector was used for sequence analysis. Graph Prism 7 was used for data analysis and for graph generatation. In addition, We used cellranger (v3.0.2) from 10X Genomics for single-cell UMI quantification and TCR clonotype assembly. We used Seurat (v3.1.2) an R package to analyze single cell RNA-seq data and to identify differentially expressed genes; graphs were created using R language. For bulk-RNA seq analysis we used kallisto (v.0.46) to map sequence reads to Mus musculus transcriptome (GRCm38/ Ensembl release 99). Kallisto TPM values were converted to absolute counts using tximport (v1.12.3) R package and DESeq2 (v.1.24.0). For differential gene expression analysis in the bulk RNA sequencing experiments we used kallisto (v.0.46) to map sequence reads to Mus musculus transcriptome (GRCm38/ Ensembl release 99). Kallisto TPM values were converted to absolute counts using tximport (v1.12.3) R package and DESeq2 (v.1.24.0) 1 was utilized for differential expression analysis. Differentially expressed genes were defined by having an adjusted p-value < 0.05 and | logFC| > log2(1.5). Im the Venn diagrams common differentially expressed genes also had common behaviour between groups. ie up and down between the two data sets. Hierarchical clustering was based on combined data from three experimental repeats. Hierarchical clustering done based on data from the individual repeats gave similar results. For Single-cell RNA-Seq analysis we used cellranger (v3.0.2) 10X Genomics for single-cell UMI quantification and TCR clonotype assembly. Hashtags oligos (HTOs) UMI counts were processed using CITE-Seq-Count (v1.4.0). We used Seurat (v3.1.2) 2,3, an R package to analyze single cell RNA-seq data, to identify differentially expressed genes. Genes expressed in at least 10 percent of all cells belonging to clones exhibiting expansion or contraction, with the adjusted p-value by Bonferroni correction less than 0.05 and with |average logeFC| > loge(1.1) were selected as statistical significant differentially expressed genes. To define Tfh clonal behaviors we used multiple binomial tests to interrogate whether the frequency of cells of a specific clone in the second timepoint is greater or less than expected, according to the frequency of the same clone in the first timepoint. Adjusted p-values (q-value) were calculated using the false discovery rate (FDR) correction. Expanded clones were defined as having cell frequency greater than expected in the second timepoint (q-value<0.05), while contracted clones were defined as having cell frequency less than expected in the second timepoint (q-value<0.05). Clones without statistical significance for any test were classified as conserved clones.

The data discussed in this publication have been deposited in NCBI's Gene Expression Omnibus (Edgar et al., 2002) and are accessible through GEO Series accession number GSE147182 (https://www.ncbi.nlm.nih.gov/geo/query/acc.cgi?acc=GSE147182)

For manuscripts utilizing custom algorithms or software that are central to the research but not yet described in published literature, software must be made available to editors/reviewers. We strongly encourage code deposition in a community repository (e.g. GitHub). See the Nature Research guidelines for submitting code & software for further information.

Data

Policy information about availability of data

All manuscripts must include a data availability statement. This statement should provide the following information, where applicable:

- Accession codes, unique identifiers, or web links for publicly available datasets
- A list of figures that have associated raw data
- A description of any restrictions on data availability

-GSE147182

Field-specific reporting

Please select the one below that is the best fit for your research. If you are not sure, read the appropriate sections before making your selection.

☒ Life sciences ☐ Behavioural & social sciences ☐ Ecological, evolutionary & environmental sciences

For a reference copy of the document with all sections, see nature.com/documents/nr-reporting-summary-flat.pdf

Life sciences study design

All studies must disclose on these points even when the disclosure is negative.

Sample size	The sample size of mice that were used per group/condition was not predetermined by statistical analysis but instead standard numbers that are accepted by the field. The number of mice used in each case allowed for rigorously testing of experimental hypothesis by appropriate statistical analysis to test the null hypothesis, minimize the probability of a false finding. Animal numbers also had to limited in accordance with the 3R's and ARRIVE guidelines, as to reduce the number of animals used to meet scientific objectives.
Data exclusions	Data only excluded for technical reasons, first bulk B cell RNA seq was excluded and repeated due to contaminants as observed by referee or if cells had died prior to adoptive transfer into host recipients.
Replication	Each experiment was repeated independently a minimum of two times and is stated in the Figure Legends. The bulk T cell RNAseq experiment was sequenced once, however was statistically powerful due the group size per condition. The 10xCiteSeq scRNAseq was repeated twice amd a total of 6 mice were used to track clonal evolution longitudionally in the same individuals. All repeats were successful apart from one adoptive transfer experiment, where the experiment was ended prematurely due to a technical issue with the viability of the cells being delivered due to suspected overly harsh treatment during their isolation.
Randomization	Litter mate controls were used for in house strain and randomly assigned to groups. Otherwise out of house, C57BL/6 wild type mice were purchased from The Jackson and divided into sex matched and age matched groups.
Blinding	Mice were homogenous in sex and age prior to grouping. Investigators were not blinded in this study (as is accepted in the field) as blinding is not needed for a scientifically sound result. For mouse experiments it is required to provide a cage label for each experimental cage detailing the conditions each individual mouse has received, and each mouse needs to be identifiable with a ear marking, which prevents blinding in such experiments.

Reporting for specific materials, systems and methods

We require information from authors about some types of materials, experimental systems and methods used in many studies. Here, indicate whether each material, system or method listed is relevant to your study. If you are not sure if a list item applies to your research, read the appropriate section before selecting a response.

Materials & experimental systems

n/a	Involved in the study
☐	☒ Antibodies
☐	☒ Eukaryotic cell lines
☒	☐ Palaeontology
☐	☒ Animals and other organisms
☒	☐ Human research participants
☒	☐ Clinical data

Methods

n/a	Involved in the study
☒	☐ ChIP-seq
☐	☒ Flow cytometry
☒	☐ MRI-based neuroimaging

Antibodies

Antibodies used

Antibody/Dilution

anti-mouse Ki67, Alexa Fluor 488, Clone B56, Cat 558616, Lot 9123835, BD 1/100
anti-mouse TCR D011.10 FITC, Clone KJ1-26, Cat 118506, Lot B192696, Biolegend 1/200
anti-mouse CD62L PECY7, Clone MEL-14, Cat 104418, Lot B269976, Biolegend 1/200
anti-mouse CD4 BUV395; Clone GK1.5, Cat 563790, Lot 9275330, BD 1/200
anti-mouse Bcl6 PE, Clone K112 91, Cat 561522, Lot 8233984, BD 1/100
anti-mouse Vβ 5.1, 5.2 T-Cell Receptor PE, Cat 553190, Lot 8345781, BD 1/200
Biotin Rat anti-mouse CD185 (CXCR5), Cat 145510, Lot B21465, BD 1/100
anti-mouse CD44 APC, Clone IM7, Cat 563058, Lot B265921, BD 1/200
anti-mouse Ki-67 FITC, Clone B56, Cat 558616, Lot 9123835, Biolegend 1/100
anti-mouse Ki-67 PE, Clone 16A8, Cat 652403, Biolegend 1/100
anti-mouse CD4, Clone RM4-5, Cat 100516, Lot B277608, Biolegend 1/200
anti-mouse CD69 Pacific Blue, Clone H1.2F3, Cat 104524, Lot B287574, Biolegend 1/200
anti mouse CD69-FITC,Clone H1.2F3, Cat 104506, Lot E031177, Biolegend 1/200
anti-CD45.2 Mouse Monoclonal Antibody PE, Clone 104, Cat 109808, Lot B271929, Biolegend 1/200
anti-mouse CD185 (CXCR5) BViolet 421™, Clone L138D7, Cat 145512, Lot B265666, Biolegend 1/100
anti-mouse TCR Vα2, Clone B20.1, Cat 127807, Lot B245807, Biolegend 1/200
anti-CD45.1 Mouse Monoclonal Antibody 110738 Biolegend 1/200
anti-mouse/human CD44 Brilliant Violet 421™, Clone IM7, Cat 103040, Lot B273304, Biolegend 1/200
anti CD44, Clone IM7, Cat 11-0441-82, eBioscience 1/200
anti-mouse CD43 PE Antibody, Clone S7, Cat 553271, Lot 7297616, Biolegend 1/200
anti-mouse CD4 APC, Cat 100516, Lot B277608, Biolegend 1/200
anti-mouse TCR DO11.10, Clone KJ1-26, Cat 118508, Lot B192696, Biolegend 1/200
anti-mouse CD38, Clone 90/CD38, Cat 553764, BD Bioscience 1/100
anti-mouse PD1 PE, Clone J43, Cat 551892, Lot 7086579, BD Bioscience 1/200
anti-mouse CD4 PE, Clone GK1.5, Cat 100408, Lot B266388, Biolegend 1/200
anti-mouse CD45.2, Clone 104, Cat 109808, Lot B271929, eBioscience 1/200
anti-mouse TCR VB5.1, Clone MR9-4, Cat 139504, Biolegend 1/200
anti-mouse CD44, Clone IM7, Cat 103027, Biolegend 1/200
anti-mouse PD1- BV711, Clone 29F.1A12, Cat 135231, Lot B298663, Biolegend 1/200
anti-mouse GL7 PB, Clone GL7, Cat 144614, Lot B306510, Biolegend 1/200
anti-mouse GL7 FITC, Clone GL7, Cat 144603, Biolegend 1/200
anti-mouse CD44 BV605, Clone IM7, Cat 563058, BD 1/200
anti-NK-1.1 Mouse Monoclonal Antibody PE, Clone PK136, Cat 557391, Lot 65616, Biolegend 1/200
anti-mouse CD38 Pacific Blue, Clone T10, Cat 102719, Biolegend 1/100
anti-mouse/human PE CD45R/B220 Antibody, Clone RA3-6B2, Cat 103208, Biolegend 1/200
anti-mouse CD86 APC, Clone GL-1, Cat 4332810, Biolegend 1/100
anti-mouse CD279 APC, Clone 29F.1A12, Cat 109112, Lot B248540, Biolegend 1/200
anti-mouse Active Caspase, Clone C92-605, Cat 561011, Lot 4318875, BD 1/100
B-Phycoerythrin, Cat AS-82001, Lot 164-119, Anaspec 50ul of 4mg/ml B-PE in 150ul of PBS
Anti-B-Phycoerythrin Rabbit, Number 100-4199, Rockland 100ug of 10mg/ml
DAPI solution, Cat 564907, Lot 9294998 10ug/ml
anti-mouse CD45.1 PE/Cyanine7, Clone A20, Cat 110729, Biolegend 1/200
TotalSeq™-C0301 anti-mouse Hashtag 1 Antibody 155861, Biolegend 1 µg
TotalSeq™-C0302 anti-mouse Hashtag 2 Antibody 155863, Biolegend 1 µg
TotalSeq™-C0303 anti-mouse Hashtag 3 Antibody 155865,Biolegend 1 µg
TotalSeq™-C0304 anti-mouse Hashtag 4 Antibody 155867,Biolegend 1 µg
TotalSeq™-C0305 anti-mouse Hashtag 5 Antibody 155869, Biolegend 1 µg

Validation

All fluorescent antibodies validated on the manufacturers website.

Eukaryotic cell lines

Policy information about cell lines

Cell line source(s)	OTII (in house) 293-6E (ThermoFisher)
Authentication	none.
Mycoplasma contamination	negative
Commonly misidentified lines (See ICLAC register)	None used

Animals and other organisms

Policy information about studies involving animals; ARRIVE guidelines recommended for reporting animal research

Laboratory animals	C57BL/6, Do11.10, OTII, Fucci, SellCreERT2 ROSAtdT, C7, F1 (C57BL/6 x Balbc). All mice used were between 6-10 weeks of age and groups were age and sex matched. Mice were housed at a temperature of 72 °F and humidity of 30–70% in a 12-h light/dark cycle with ad libitum access to food and water. Male and female mice aged 8–10 weeks at the start of the experiment were used throughout.
Wild animals	No wild animals were used in this study.
Field-collected samples	none
Ethics oversight	All procedures in mice were performed in accordance to protocols approved by the Rockfeller University IACUC. All animal experiments were performed according to the protocols approved by the Institutional Animal Care and Use Commitee of NIAID, NIH.

Note that full information on the approval of the study protocol must also be provided in the manuscript.

Flow Cytometry

Plots

Confirm that:

☒ The axis labels state the marker and fluorochrome used (e.g. CD4-FITC).

☒ The axis scales are clearly visible. Include numbers along axes only for bottom left plot of group (a 'group' is an analysis of identical markers).

☒ All plots are contour plots with outliers or pseudocolor plots.

☒ A numerical value for number of cells or percentage (with statistics) is provided.

Methodology

Sample preparation	Single cell suspensions were obtained from popiteal lymph nodes or spleens of experimental mice, T cells and B cells were isolated by negative selection using PE-Easy Sep selection. Otherwise untouched single cell suspensions were stained for analysis.
Instrument	BD FACSARIAII, BD FACSSYMPHONY
Software	FACSDIVA version 8.0.2, FlowJo version v10.4.2
Cell population abundance	purity was above 95%
Gating strategy	Responsing Tfh T cells were isolated by gating of live single cells that were CD4 positive, CD62 low, CD44 high, PD1 high, CXCR5 high, and tdT +.

☒ Tick this box to confirm that a figure exemplifying the gating strategy is provided in the Supplementary Information.